# A network of Notch-dependent and -independent *her* genes controls neural stem and progenitor cells in the zebrafish thalamic proliferation zone

**Christian E. Sigloch[1,2,3], Dominik Spitz[1,4], and Wolfgang Driever[1,3*]**

Affiliations

(1) Developmental Biology, Institute Biology 1, Faculty of Biology, University of Freiburg, Hauptstrasse 1, 79104 Freiburg, Germany

(2) Spemann Graduate School of Biology and Medicine SGBM, University of Freiburg, Albertstraße 19A, 79104 Freiburg, Germany

(3) Signalling Research Centres CIBSS and BIOSS, University of Freiburg, Schänzlestraße 18, 79104 Freiburg, Germany

(4) Current Address: Renal Division, Department of Medicine, Faculty of Medicine and Medical Center, University of Freiburg, 79106 Freiburg, Germany

*Correspondence should be addressed to:

Wolfgang Driever

Phone. +49-761-203-2587; Fax +49-761-203-2550

Email: driever@biologie.uni-freiburg.de

WD: ORCID-ID 0000-0002-9551-9141

Short title: HER/HES regulatory network

Key words: neurogenesis, neural stem cells, HES/HER genes, Delta-Notch signaling, neural proliferation zone, thalamus, zebrafish

## Abstract

Neural proliferation zones mediate brain growth, and employ Delta/Notch signaling and HES/HER transcription factors to balance neural stem cell (NSC) maintenance and generation of progenitors and neurons. We investigated Notch-dependency and function of *her* genes in the thalamic proliferation zone of developing zebrafish larvae. Nine Notch-dependent genes, *her2, her4.1-5, her12, her15.1-2*, and two Notch-independent genes, *her6, her9*, are differentially expressed, and define distinct NSC and progenitor populations. *her6* prominently executes patterning information to maintain NSCs and the zona limitans intrathalamica Shh signaling activity. *her6, her9* double mutants reveal that Notch-independent *her* genes predominantly regulate NSC maintenance and transition into the progenitor pool. Surprisingly, combined deletion of all Notch-dependent *her* genes does not affect NSCs or progenitor formation. Combined genetic manipulation of up to eleven Notch-dependent and -independent *her* genes revealed that Notch-dependent *her* genes may regulate progenitor progression into neurogenesis, but not progenitor generation itself. The *her* gene network is partially redundant, with Notch-independent *her* genes better substituting for loss of Notch-dependent genes than vice versa. Together, *her* gene regulatory feedback loops and crossregulation contribute to the observed robustness of NSC maintenance.


## Introduction

The zebrafish brain continually grows and adds new neurons throughout development and into adult stages, and has high capacity to regenerate neurons after injury (Kishimoto et al., 2012; Zupanc, 2001). The source of these new neurons are neural stem cells (NSCs) located in at least 16 adult neural proliferation zones (NPZs) (Grandel et al., 2006; Zupanc et al., 2005). These anatomically defined NPZs are mostly located at the ventricular wall (Adolf et al., 2006), where Hairy and Enhancer of split (HES/Her) transcription factors are expressed and regulate neurogenesis (Chapouton et al., 2011). During development, the embryonic neuroepithelium establishes highly active late embryonic and early larval proliferation zones, which develop into neural stem cell niche-like adult proliferation zones. So far, the mechanisms that balance NSC maintenance and neurogenesis in these larval NPZs are not well understood.

62 HES/Her factors in NPZs control neurogenesis by inhibiting proneural gene mediated
63 differentiation (Ishibashi et al., 1994; Kageyama et al., 2007; Sasai et al., 1992). In mice, absence
64 of the basic Helix loop Helix (bHLH) transcription factors HES1 and HES5 leads to accelerated
65 differentiation, accompanied by loss of radial glia and later-born cell types (Hatakeyama et al.,
66 2004). Moreover, in zebrafish and mouse, *Hes/her* genes were shown to be important for the
67 maintenance of local stem cell populations at boundaries that form signaling and growth centers
68 (Baek et al., 2006; Hatakeyama et al., 2004), for example the midbrain-hindbrain boundary (Geling
69 et al., 2004) and the zona limitans intrathalamica (ZLI) (Scholpp et al., 2009).

70 In *Drosophila,* the expression of *E(spl)* is Notch-dependent (Jennings et al., 1994), while the
71 expression of *hairy*, encoding a closely related bHLH factor, is directed by local patterning signals
72 (Riddihough and Ish-Horowicz, 1991). However, this strict distinction is not conserved in
73 vertebrates (Chapouton et al., 2011; Davis and Turner, 2001). In mouse, *Hes1* and *Hes5* are
74 downstream targets of Notch signaling, although *Hes1* expression and stability are the result of
75 additional Notch-independent input (Kageyama et al., 2007; Ohtsuka et al., 1999). In contrast to
76 HES1 and HES5, the transcription factor HES6 functions as a negative regulator of HES1, thereby
77 promoting differentiation (Bae et al., 2000), and its expression is controlled by proneural genes
78 (Koyano-Nakagawa et al., 2000).

79 In zebrafish, the *her* gene family expressed in NPZs is significantly expanded compared to
80 mammals (Zhou et al., 2012). Nine *Hes5* zebrafish homologs are located in two gene clusters,
81 *her4.1* to *her4.5* and *her12* on chromosome 23, and *her15.1, her15.2* and *her2* on chromosome 11.
82 There are two *Hes1* homologs, *her6* and *her9*, and four *Hes6* homologs, *hes6*, *her8a*, *her8.*2 and
83 *her13*. *her4* and *her15, her6* and *her9*, as well as *her8a* expression have been characterized in adult
84 neural stem cell (NSC) zones (Chapouton et al., 2011; Zhou et al., 2012). Zebrafish homologs of
85 *Hes1*, *Hes5* and *Hes6* have also been investigated in the neural plate during early embryonic
86 development (Bae et al., 2005; Takke et al., 1999; Webb et al., 2011). So far however, little is
87 known about potential cross-regulatory interactions or redundancies among *her* genes in NSCs and
88 during neurogenesis in larval neural proliferation zones.

89 Here, we analyzed the impact of Notch signaling and *her* family genes on expression of specific
90 *her* genes in NSCs and neural progenitor cells (NPCs) to reveal the organization of *her* gene
91 regulatory networks in neurogenesis. We focus on the highly active early larval thalamic
92 proliferation zone (TPZ) at the ventricular wall of the diencephalon in the thalamus proper (dorsal
93 thalamus), the ZLI, and the prethalamus (Mueller, 2012; Scholpp and Lumsden, 2010), together
94 constituting the thalamic complex. Based on *her* gene expression, we define distinct NSC
95 populations in the TPZ. We generated compound mutants for two Notch-independent (*her6* and

96 *her9*) and nine Notch-dependent (*her2, her4.1-5, her12, her15.1-2*) *her* genes. Based on loss-of-
97 function and overexpression experiments, we generated a model for cross-regulatory interactions
98 of Notch-dependent and -independent *her* genes in the TPZ. Our data indicate that Notch-
99 independent *her* genes are important for NSC maintenance and patterning in the TPZ. Notch-
100 dependent *her* genes however appear not strictly required for NSC maintenance but might rather
101 modulate progression of neurogenesis.

102

103

104 **Results**

105

106 ***her* family gene expression in the thalamic proliferation zones**

107 We surveyed published information (www.zfin.org; Chapouton et al., 2011; Shankaran et al., 2007;
108 Sieger et al., 2004; Zhou et al., 2012) on zebrafish *her* family genes for expression in the
109 diencephalon, and selected homologs of mammalian *Hes1* (*her6, her9*), *Hes5* (*her2, her4.1-4.5,*
110 *her 12, her15.1-15.2)* and *Hes6* (*her8a, her8.2*) for analysis of their expression patterns in the TPZ
111 by whole mount in situ hybridization (WISH; Fig. 1A-L; Fig. S1A-H). The five *her4.1-4.*5 genes
112 together with *her12* form a cluster on chromosome 23 ("*her4;12 cluster*"), while the two *her15.1-*
113 *15.*2 genes form a cluster together with *her2* on chromosome 11 ("*her2;15 cluster*"). Genes within
114 each cluster have high sequence similarity. Our *her4* probe was designed to detect expression of
115 all five *her4* genes (*her4.1-her4.5*) combined (subsequently referred to as *her4*). Similarly, our
116 *her15* probe detects *her15.1* and *her15.2* (referred to as *her15*). We focused our analysis on two
117 days (48 hours post fertilization, hpf) to four days (96 hpf) old embryos and early larvae, when the
118 TPZ is a highly active proliferation zone with a diversity of neurogenesis mechanisms involving
119 *neurog1, ascl1* and *olig2* (Scholpp et al., 2009; Virolainen et al., 2012), (see also Fig. 7C and Fig.
120 11A, B).

121 In the TPZ, *her6*, *her9*, *her4, her2,* and *her15* expression were detected with strong WISH signals.
122 *her2* is clustered with *her15.1-15.2*, and has a similar expression domain. The expression of these
123 *her* genes in the thalamic complex was mostly restricted to the wall of the diencephalic ventricle
124 and the adjacent lateral ventricle (Fig. S1A'-H').

125 In contrast, the *Hes6* homologs *her8a* and *her8.2* had weak WISH signals in the TPZ (Fig. S1C-
126 D'). *her8.2* and *her8a* are broadly expressed in neural proliferations zones at 48 hpf, but expression
127 decreases on the fourth day of development, such that at 96 hpf we could detect only low levels of

128 *her8.2* and very faint *her8a* expression in the TPZ (Fig. 1E,F,K,L and Fig. S1C-D'). *her12*
129 expression appears restricted to the hindbrain and later the midbrain-hindbrain boundary (Fig.
130 S1E,E'; Fig. S2A,G), and thus, despite being in a cluster with *her4* genes, differs significantly in
131 expression.

132 In summary, while expression of the *Hes6* homologs *her8a* and *her8.2* decreases during early TPZ
133 formation, *Hes1* (*her6, her9*) and *Hes5* (*her2, her4.1-4.5, her15.1-15.2)* homologs likely provide
134 the major *her* gene activity in the maturing TPZ.

135

136 **Notch dependency of neural *her* gene expression**

137 Regulation of zebrafish *her* gene expression by Notch signaling has been characterized during
138 embryonic stages (Pasini et al., 2004; Shankaran et al., 2007; Takke et al., 1999), but not in larval
139 NPZs. To assess Notch dependency of expression of *Hes1, Hes5* and *Hes6* homologs, we used
140 three approaches. We first analyzed *mind bomb1* (*mib1*$^{ta52b}$) mutants that lack Notch signaling due
141 to impaired internalization of the ligand Delta (Itoh et al., 2003). Second, we globally
142 overexpressed the Notch Intracellular Domain (NICD) by heat shock in 72 hpf larvae (Scheer and
143 Campos-Ortega, 1999). Third, we treated larvae with the Notch inhibitor LY-411575
144 (Rothenaigner et al., 2011).

145 The *Hes1* homologs *her6* and *her9* are still expressed at largely normal levels in *mib1*$^{ta52b}$ mutant
146 embryos (Fig. 1A-B'), and NICD overexpression only slightly increased *her9* and hardly at all *her6*
147 expression (Fig. 1G-H'). Upon Notch inhibitor treatment, *her6* and *her9* expression continued,
148 albeit at slightly reduced levels (Fig. 1M-N'). These experiments demonstrate *her6* and *her9*
149 expression to be Notch-independent at analyzed larval stages.

150 In contrast, the expression of *Hes5* (*her2, her4, her12* and *her15*) and *Hes6* (*her8a* and *her8.2*)
151 homologs is lost in *mib1*$^{ta52b}$ mutants (Fig. 1C'-F', Fig. S2A-D'). The ectopic *her15* expression in
152 the tectum of *mib1* mutants appeared very different from the expression in wild type (WT; Fig.
153 1D,D'), and may reflect dysregulation. Expression of *Hes5* homologs was strongly induced by
154 NICD, while the *Hes6* homologs showed only a moderate increase in expression (Fig. 1I-L'). Upon
155 Notch inhibitor treatment, expression of *Hes5* and *Hes6* homologs was nearly absent (Fig. 1O-R';
156 Fig. S2G-I'), except *her2*, which was expressed at reduced levels after LY-411575 treatment (Fig.
157 S2J,J'). These findings suggest that, while *her2* and *her15* are located in the same cluster, *her15* is
158 mostly Notch-dependent while *her2* may be only partly controlled by Notch.

159 To conclude, in the TPZ of 3-4 dpf larvae, expression of the *Hes1* homologs *her6* and *her9* are only
160 weakly affected by perturbation of Notch signaling and are hereafter referred to as Notch-

161 independent. In contrast, *her4* and *her15* expression are strictly dependent on Notch signaling.
162 Given that *her8a* and *her8.2* have only low and declining levels of expression in the TPZ on the
163 fourth day of development, we did not include these two genes in our further analysis.

164

165 **Differential expression of *her* genes in the thalamus proper, prethalamus and ZLI**

166 We next investigated by fluorescent WISH whether Notch-dependent and Notch-independent *her*
167 genes are differentially expressed in the TPZ (Fig. 2). *her4* and *her6* expression was mostly
168 restricted to the periventricular TPZ wall, and largely co-expressed with the NSC marker *sox2* (Fig.
169 S3A-B''). During early development, *her6* is expressed in the presumptive thalamic complex
170 (Scholpp et al., 2009). During larval development, *her6* expression is absent from the ZLI, but
171 maintained in the rostral thalamus and prethalamus (Fig. 2A,A',F; Scholpp and Lumsden, 2010).
172 At the ventricle along the midline, *her4* is strongly expressed where *her6* is absent, namely in the
173 ZLI, caudal thalamus (cTh) and the pretectum (Fig. 2A). In the caudal thalamus, *her4* is also
174 expressed laterally adjacent to the ventricular wall (Fig. 2A'). *her4* and *her15* were mostly co-
175 expressed in the ZLI, caudal thalamus and pretectum (Fig. 2B,B'; for comparison, chromogenic
176 *her4* WISH in Fig. 2G). *her9* was expressed only weakly in the ZLI and the cTh, and both *her6*
177 and *her9* were expressed in rather non-overlapping territories (Fig. 2C,C´). We also directly
178 compared the expression of both Notch-dependent *her4* and *her15* with Notch-independent *her6*
179 and *her9* combined, using pairwise mixed probes, and found that their expression domains together
180 covered the whole ventricular zone of the thalamic complex (Fig. 2D-D''').

181 Looking at combined expression domains, *her4, her15,* and, to a lesser extent, *her9* are co-
182 expressed in the ZLI and the caudal thalamus, while *her6* is selectively expressed in prethalamus
183 and rostral thalamus (Fig. 2F). Thus, interestingly, Notch-independent *her9* is expressed in the
184 same anatomical area as the Notch-dependent *her4* and *her15*, while the second Notch-independent
185 gene *her6* is expressed in largely exclusive territories devoid of other *her* gene expression.

186 When we analyzed *her4, her6,* and *her9* by triple fluorescent HCR at cellular resolution in the
187 thalamus (Fig. S4), we realized that domains of high expression of each gene at the ventricle are
188 mostly exclusive. In addition, in cells which may correlate to neural progenitors, we detected *her4*
189 expression at lower level distant from the high *sox*2 expressing ventricular NSCs. To validate this
190 hypothesis, we used triple fluorescent HCR to analyze *sox2, ascl1b,* and *neurog1* expression in the
191 same anatomical region (Fig. S5; Movie M1). The data show high *sox2* expressing cells ($Sox2^{high}$)
192 at the ventricular walls largely devoid of *ascl1b* and *neurog1* expression, corresponding to NSCs.
193 In addition, we find a *sox2* low expressing domain ($Sox2^{low}$) in the region corresponding to low

194 *her4* expression, which also expresses *ascl1b* or *neurog1*, and thus are neural progenitor cells
195 (NPCs) in early neurogenesis.

196 Next, we analyzed *her4, her6* and *her9* in relation to proneural gene expression in the Sox2$^{low}$ NPC
197 region (Fig. S6). We observe that in this domain, *neurog1* expression largely overlaps with *her4*
198 expression, but not with *her6* and *her9.* Similarly, expression of *ascl1a/b* is largely exclusive from
199 the *her6* expressing regions (Fig. S6D). *ascl1a/b* expression overlaps widely with *dla* expression
200 in the Sox2$^{low}$ *her4* region (Fig. S6E), suggesting that Delta and Notch-dependent *her* genes control
201 *neurog1* and *ascl1a/b* in the NPC region. To investigate in more detail the relation of Delta
202 signaling and *her* genes in NSC and NPC regions, we analyzed combined expression of *dla* with
203 *sox2, her4, her6* and *her9* (Fig. S7). Surprisingly, *dla* expression appears higher in the NPC Sox2$^{low}$
204 region than in the Sox2$^{high}$ ventricular zone (Fig. S7A). *her4* and *dla* expression largely overlap in
205 the NPC region (Fig. S7B). In contrast, regions with highest levels of *her6* and *her9* expression are
206 devoid of *dla* expression (Fig. S7C-D).

207 In conclusion, our data identify at least three fundamentally distinct *her* expressing cell populations
208 in the TPZ (Fig. 11A,B): (1) Sox2$^{high}$ NSCtype1 at the ventricular wall with predominant
209 expression of Notch-independent *her6*, and absent *dla*; (2) Sox2$^{high}$ NSCtype2 at the ventricular
210 wall with high expression of Notch-dependent *her4* and/or *her15*, low *her9* expression, and in most
211 regions *dla* expression. However, *her6* expression is absent from these regions; (3) Sox2$^{low}$ NPCs
212 away from the ventricular wall with *dla* expression, either *ascl1b* or *neurog1* expression, and low-
213 level expression of Notch-dependent *her4*.

214

215 **Auto- and cross-regulation of Notch-independent *her* genes**

216 Given the exclusive expression domains in the TPZ, we tested genetically whether *her6* and *her9*
217 might cross-repress each other. We used CRISPR/Cas9 to delete large parts of the bHLH domains
218 of *her6* and *her9*, and isolated mutant alleles with premature stop codons that leave the remaining
219 aminoterminal peptides non-functional (Fig. 3A, B). We analyzed genetic interactions in *her6* and
220 *her9* single and double mutants (Fig. 3C-N) using WISH probes that detect the shortened mutant
221 transcripts. At 48 hpf, *her6* expression levels in several regions appear enhanced in *her6* mutants,
222 and even stronger in *her6, her9* double mutants, while *her6* expression in *her9* mutants appears
223 similar to WT in most brain regions (Fig. 3C-F'). Upregulation of *her6* in double mutants is even
224 stronger at 96 hpf (Fig. 3G-H'). *her9* expression levels in *her6* and *her9* single and double mutants
225 at 48 hpf appear not strongly affected, while *her9* expression at 96 hpf is slightly increased in
226 double mutants (Fig. 3I-N'). To quantify potential cross-regulations independently, we also

227 analyzed *her6* and *her9* mRNA levels by qPCR on genotyped 4 dpf embryonic heads. We found a
228 significant upregulation of *her6* transcripts in *her6* mutants and of *her9* transcripts in *her9* mutants
229 (Fig. 3O; p-values see Supplementary Table 5), indicating negative autoregulation. We next asked
230 whether *her6* and *her9* cross-regulation is redundant, and analyzed *her6*, *her9* double mutants.
231 Upregulation of *her6* and *her9* transcripts in *her6*, *her9* double mutant was significantly stronger
232 than in single mutants (Fig. 3O). We conclude that *her6* and *her9* exert negative cross-regulation
233 on each other, partially redundant with negative autoregulation. In fact, as revealed from lower
234 *her6* expression in *her9* than in *her6* mutants, and from lower *her9* expression in *her6* than in *her9*
235 mutants, negative autoregulation appears stronger than cross-regulation. Nevertheless, the strong
236 upregulation of *her6* and *her9* in double mutants reveals a significant contribution of negative
237 cross-regulation.

238

239 **Combined loss of *her6* and *her9* activity affects neural stem cells, progenitor cells and ZLI**

240 We further analyzed *her6*, *her9* double mutants to determine the impact of loss of Notch-
241 independent *her* gene function on NSCs, progenitors, and cell proliferation in the TPZ. We used
242 an anti-Sox2 antibody to mark NSCs by whole mount immunofluorescence (Fig. 4A-D'' and
243 Movie M2). In WT larvae, Sox2 positive nuclei lined the thalamic ventricular walls, including the
244 lateral ventricle away from the midline, and nuclei with lower Sox2 immunoreactivity ($Sox2^{low}$)
245 were also detected in subapical positions adjacent to the cell layer that forms the ventricular wall
246 (Fig. 4A' and cutout in $A_1$). In the *her6*, *her9* double mutants, the subapical $Sox2^{low}$ cell nuclei
247 were strongly reduced or missing, and $Sox2^{high}$ cell nuclei restricted to the ventricular wall (Fig.
248 4B' and $B_1$; *her9* and *her6* single mutants each have largely normal distribution of Sox2 positive
249 nuclei, data not shown). In addition, the lateral extension of $Sox2^{high}$ nuclei along the lateral
250 expansion of the ventricle was strongly reduced, indicating a loss of ventricular NSCs (Fig. 4A''
251 and B'', white arrowheads and Movie M2).

252 To determine whether the loss of Sox2 positive cells may correlate with reduced cell proliferation,
253 we used an anti-phospho-Histone H3 (pH3) antibody to detect cells in mitosis. Compared to WT,
254 *her6, her9* double mutants had a similar distribution of pH3 positive mitotic nuclei in the TPZs
255 ventricular zone (Fig. 4A',B' and Movie M2; nuclei not counted). However, pH3 positive nuclei
256 in *her6, her9* double mutants were largely absent in the lateral ventricle region, which is also devoid
257 of Sox2 positive cells. *ccnd1* expression, which accumulates during G1 to S phase transition, was
258 reduced in the TPZ especially along the lateral ventricle of *her6, her9* double mutants (Fig. S8).
259 Thus, while mitotic activity of $Sox2^{high}$ TPZ cells is not impaired, there are no mitotically active
260 cells observed in the lateral ventricle wall devoid of $Sox2^{high}$ cells.

261 Next, we investigated proneural gene expression in the Sox2$^{low}$ NPCs in the TPZ. Fluorescent
262 HCR-RNA FISH shows that *sox2* in Sox2$^{low}$ regions is co-expressed with proneural genes (Fig.
263 4C-C''). The strongest co-expression is in the thalamus proper in Sox2$^{low}$ expressing cells that are
264 not in direct contact with the ventricle (Fig. S5A-F and Movie M1). Here, *sox2* expression was
265 overlapping with *neurog1* or *ascl1b* in Sox2$^{low}$ NPCs. More precisely, *ascl1b* is expressed in a
266 narrow stripe in the rostral thalamus, while *neurog1* is expressed in the caudal thalamus (Fig. 4C-
267 C''; *ascl1a* is also expressed in prethalamus and pretectum, see also Fig. 11A-C). In *her6*, *her9*
268 double mutants however, *neurog1* and *ascl1b* expression domains were intermingled (arrowheads)
269 and the area of expression is smaller and narrower (Fig. 4D-D''). Taken together, we found *her6,*
270 *her9* double mutants to have a smaller domain of *sox2$^{low}$* expressing progenitors, and lack the
271 proper spatial organization of *neurog1* and *ascl1b* NPCs.

272 Next, we tested whether loss of Sox2 positive NSCs may correlate with changes in the ZLI. In WT,
273 *shha* in the thalamus is expressed in the basal plate and the ZLI (Scholpp and Lumsden, 2010). As
274 development progresses, *shha* expression is maintained medially in close proximity to the ventricle
275 and expands dorsally into the ZLI, where the expression extends along the walls of the lateral
276 ventricle (Fig. 5A-D,I). While at 24 hpf the *shha* expression in the ZLI appears largely normal in
277 *her6, her9* double mutants (Fig. 5A,A',E,E'), at 72 hpf and 96 hpf we observe a progressive loss
278 of the *shha* expression domain that normally demarcates the ZLI separating the prethalamus from
279 the thalamus proper, both in its lateral and dorsal domains (Fig. 5). A partial loss of *shha* expression
280 along the lateral ventricular walls was also observed in the ZLI of *her6* single mutants (Fig. S9),
281 although the extent of loss of *shha* expression in this region varied among larvae (Fig. S9C' and
282 D', white arrowheads). We interpret this variability as gradual loss of the ZLI cell population that
283 forms this *shha* expression domain.

284

285 **Loss of the two Notch-dependent *her* gene clusters does not affect NSCs and NPCs in the TPZ**

286 The two *her4;12* and *her2;15* gene clusters active in the TPZ contain nine *Hes5* zebrafish homologs
287 (Zhou et al., 2012), but no other genes (www.ensembl.org, accessed on 30. August 2021). To
288 genetically inactivate these nine *her* genes, we generated large precise deficiencies in both
289 chromosomal regions (Fig. 6A,B and Fig. S10). The 28 kb deficiency
290 *Df(Chr23:her12,her4.1,her4.2,her4.3,her4.4,her4.5)m1364* or *m1365*, abbreviated here as
291 *Df(her4;12)*, and the 30 kb deficiency *Df(Chr11:her2,her15.1,her15.2)m1490*, abbreviated here as
292 *Df(her2;15)* were generated using the CRISPR/Cas9 system. The deletions were confirmed by
293 sequencing (Fig. S10). WISH for *her4* and *her15* demonstrated that there were no transcripts left
294 in theses mutants, and no translocations of the deleted sequences occurred (Fig. 6C-D').

295 We could not observe any morphological changes in *Df(her4;12)* or *Df(her2;15)* mutant larvae
296 until 30 dpf (data not shown) or in fixed 3 dpf larvae. Therefore, we generated larvae devoid of all
297 nine Notch-dependent *her* genes in crosses of *Df(her4;12)*, *Df(her2;15)* double deficiency
298 heterozygous parents. Surprisingly, double deficiency homozygous larvae also appeared
299 morphologically largely normal. To assess whether thalamic neurogenesis may be affected, we
300 analyzed *neurog1* expression and found it also unchanged (Fig. 6E-F'). To determine whether the
301 NSC compartment was affected in these mutants, we performed immunofluorescence for Sox2 and
302 pH3 (Fig. 7A-B'' and Movie M3). The distribution of pH3 positive nuclei appeared unchanged in
303 *Df(her4;12)*, *Df(her2;15)* double mutants compared to WT embryos (Fig. 7A-B'') and the
304 expression of *ccnd1* was unchanged (Fig. S8), suggesting normal proliferation in the TPZ. The
305 $Sox2^{high}$ nuclei layer covering the ventricular wall of the thalamus proper appeared intact (small
306 arrow in Fig. $7A_1$,$B_1$), and also the adjacent subapical $Sox2^{low}$ nuclei appeared normal (arrowhead
307 in Fig. $7A_1$,$B_1$). The shape of the nuclei at the ventricular wall was spherical, and the subapical
308 $Sox2^{low}$ nuclei were elongated, both in WT and *Df(her4;12)*, *Df(her2;15)* double mutants. $Sox2^{high}$
309 nuclei lined the lateral ventricle along its full lateral extent (Fig. 7A'' and B'' arrowheads). Thus,
310 NSCs appear to develop normally in the TPZ devoid of Notch-dependent *her* genes.

311 We also analyzed *her* gene expression in *her6*, *her9* and in *Df(her4;12)*, *Df(her2;15)* double
312 mutants (data not shown). *her6* and *her9* expression is largely unaffected in *Df(her4;12)*,
313 *Df(her2;15)* double mutants in line with their Notch-independent regulation. Based on WISH, *her4*
314 and *her15* expression appear slightly increased in the NPC area of *her6* and *her9* double mutants,
315 but at the ventricular wall *her4* and *her15* expression do not invade into the *her6* expression
316 domains in the rostral thalamus and prethalamus (data not shown), suggesting that mechanisms
317 other than repression by *her6* limit *her4* and *her15* expression in these domains.

318 To determine whether also progenitor cells appear normal, we analyzed expression of *neurog1*,
319 *ascl1a/b* and *olig2*. *olig2* is expressed in a stripe of cells parallel to the ventricular wall, adjacent to
320 the expression of *neurog1* (Fig. 7C-C'', arrowheads). Both the *olig2* and *neurog1* expression
321 domains appeared unchanged in *Df(her4;12)*, *Df(her2;15)* double deficiency mutants (Fig. 7D-D'',
322 arrowheads). Additionally, thalamic *ascl1a/b* expression domains appeared normal in double
323 deficiency mutants (white arrows). Although more subtle changes in expression cannot be
324 excluded, the periventricular stem and progenitor cell compartments of the TPZ appeared very
325 similar to WT. Thus, surprisingly, in the absence of most Notch-dependent *her* genes, NSC and
326 NPC populations appear unaffected. This is in stark contrast to the defects observed in the *her6*,
327 *her9* double mutant.

328

329 **Her4 and Her6 overexpression reveal selective cross-regulation of *her* genes**

330 We next analyzed potential cross-regulation between Notch-dependent and -independent *her* genes
331 by heat shock driven overexpression of Her4 or Her6 using *Tg(hsp:her4-FLAG)* and *Tg(hsp:her6-*
332 *FLAG)* transgenic lines. When *Tg(hsp:her4-FLAG)* larvae were analyzed by WISH 2.5 hours post
333 heat shock, *her4* was confirmed to be overexpressed (Fig. 8A,A'), and we detected downregulation
334 of *her15* expression (Fig. 8B,B'). Her4 overexpression however did not affect the expression levels
335 of *her6* and *her9* (Fig. 8C-D'). In contrast, overexpression of Her6 strongly downregulated *her9*
336 and both *her4* and *her15* (Fig. 8E-H'). This suggests that Notch-independent *her* genes negatively
337 cross-regulate Notch-dependent *her* gene expression, while Notch-dependent *her* genes negatively
338 cross-regulate other Notch-dependent *her* genes, but do not cross-regulate Notch-independent *her*
339 gene expression.

340

341 **Overexpression of Her6, but not Her4, strongly downregulates proneural gene expression**

342 We next tested whether Her4 or Her6 might differentially regulate proneural gene expression by
343 heat-shock driven overexpression at 70 hpf and fixation 2 hours after heat shock. Upon Her4
344 overexpression, surprisingly, *neurog1* expression appeared largely unchanged, while *ascl1b*
345 expression was reduced in 9 out of 14 larvae (Fig. 9A-B'). This finding is surprising, because a
346 strong effect of Notch-dependent *her* genes on proneural gene expression would be expected
347 (Imayoshi et al., 2013; Takke et al., 1999). *neurod1* and *neurod6b* expression were unchanged two
348 hours after *her4* heat shock (Fig. 9C-D'). *sox2* expression was slightly reduced in 9 out of 15 *her4*
349 heat shocked larvae (Fig. 9E-E'). In contrast, overexpression of Her6 strongly downregulated
350 expression of *neurog1* and *ascl1b*, and, to a lesser extent, also of the late progenitor markers
351 *neurod1* and *neurod6b* (Fig. 9F-I'). In addition, expression of the stem cell marker *sox2* appeared
352 slightly reduced in 11 of 15 Her6 heat shock larvae (Fig. 9J-J'), but more strongly affected than by
353 heat-shock overexpressed Her4. We also tested whether overexpression of Her4 or Her6 might
354 have a prolonged effect on proneural gene expression late after heat shock. We analyzed larvae 6
355 hours after beginning of the 30 min heat shock and found *neurog1* and *ascl1b* expression at normal
356 levels (Fig. S11A-D'). Since *her6* consistently downregulated *neurog1* and *ascl1b* 2.5 hrs after heat
357 shock, their expression appears to be back to normal only a few hours after overexpression of *her6*
358 ends. This suggests that the NSC regulatory network is robust against perturbations in Her6
359 expression level, and rapidly re-establishes normal activity. Together, our findings reveal a strong
360 regulatory impact of Her6 on progenitors and stem cells, and indicate that Notch-independent Her6
361 might be a much more potent inhibitor of neurogenesis compared to Notch-dependent Her4.

362

363 **Combined loss of activity of eleven Notch-dependent and -independent *her* genes**

364 We next asked whether Notch-dependent and -independent *her* genes may functionally compensate
365 for each other despite their different regulation. We genetically combined the two deficiencies
366 eliminating all nine *Hes5* homologs together with mutant alleles of *her6* and *her9,* and named
367 embryos homozygous mutant for all eleven *her* genes "*her* undecimal mutants" (*her*UDM; for
368 *Df(her4;12), Df(her2;15), her6, her9*). The brains of *her*UDM embryos appeared severely
369 malformed, and embryos did not survive beyond 5 dpf. When analyzed at 56 hpf (Fig. 10A-B'),
370 *her*UDM embryos had the most severe morphological defects in neural tissues that undergo
371 significant expansion by proliferation on the second day of development, such as the cerebellum,
372 the ventral part of the retina, and the rhombic lip. Early forming neural tissues however appeared
373 largely normal, which might be due to compensation by other *her* genes expressed during early
374 stages of development, including *her3*, *her8a and her8.2* (Onichtchouk et al., 2010; Webb et al.,
375 2011).

376 We analyzed Sox2 expression in *her*UDM embryos and observed a severe but quite variable overall
377 phenotype, ranging in the TPZ from strong reduction of both the Sox2$^{high}$ NSC and the Sox2$^{low}$
378 NPC compartments (as shown in Fig. 10D-D'') to extreme anatomical malformations rendering
379 analysis of the TPZ difficult (not shown). The Sox2$^{high}$ expressing nuclei in 3 dpf *her*UDM embryos
380 along the ventricular wall appeared disorganized compared to WT in that the ventricular layer of
381 Sox2$^{high}$ nuclei was interrupted (Fig. 10C-D'' and Movie M4), and some Sox2 positive nuclei were
382 displaced from the ventricular wall, suggesting that the epithelial integrity of the ventricle may be
383 impaired (Fig. 10$C_1$ and $D_1$, arrows). Similar loss of neuroepithelial integrity had been reported for
384 *Hes1, Hes5* double mutant mice (Hatakeyama et al., 2004). In the lateral view, it appeared as if
385 there were less Sox2 positive nuclei lining the ventricle wall, which might however also reflect the
386 altered shape of the ventricle in the mutant (Fig. 10C,D). Similar to *her6*, *her9* double mutants, the
387 Sox2$^{low}$ nuclei located subapically away from the ventricular wall of the thalamus proper were
388 nearly absent and did not show the elongated shape typical for WT NPCs (Fig. 10$C_1$,$D_1$,
389 arrowheads). The layer of Sox2$^{high}$ nuclei observed in WT along the walls of the lateral ventricle
390 was completely missing (Fig. 10C'',D''). In the diencephalon of *her*UDM embryos we still
391 detected pH3 positive nuclei at the ventricular walls (Fig.10D' and Movie M4), suggesting that
392 NSC proliferation is not completely eliminated.

393 We tested whether a single WT allele of a Notch-dependent or -independent *her* gene may rescue
394 the *her*UDM phenotype. A single WT allele of the *her2;her15* gene cluster in *Df(her4;12)*
395 homozygous, *Df(her2;15)* heterozygous, *her6*$^{-/-}$, *her9*$^{-/-}$ mutant larvae did partially rescue the

396 *her*UDM phenotype (Fig. 10E-E'' and Movie M5, right). The integrity of the ventricular wall as
397 defined by Sox2$^{high}$ cells was restored and resembled the phenotype in *her6*, *her9* double mutants
398 (Fig. 10E$_1$, arrow, E'', and Movie M5). Like in the *her6*, *her9* double mutant, the subapical Sox2$^{low}$
399 positive nuclei were still missing (Fig. 10E$_1$, arrowhead and Movie M5). In contrast, a single *her6*
400 WT allele in *Df(her4;12), Df(her2;15), her6$^{+/-}$, her9$^{-/-}$* mutant larvae fully restored the Sox2
401 expressing nuclei along the lateral ventricular wall (Fig. 10F'' arrowhead, and Movie M5, left).
402 The ventricular epithelium appeared intact (Fig. 10F$_1$, arrow), and the subapical Sox2$^{low}$
403 immunoreactive NPC nuclei were present and had the normal elongated nuclear shape (Fig. 10F'
404 and F$_1$, arrowhead). Individual effects of *her9* or *her4,12* were not tested, because they are tightly
405 linked on the *her9 $^{m1505}$, Df(her4;12)* chromosome 23 we used.

406 In summary, the *her*UDM phenotype revealed that, first, the eleven *her* genes analyzed provide
407 most if not all of the Her activity in the TPZ at 3-4 dpf, given the severe loss of NSCs and NPCs.
408 Second, Notch-dependent and -independent *her* genes appear to act partially redundant in NSC
409 maintenance. Third, the Notch-independent *her6* makes the most predominant contribution to NSC
410 and NPC maintenance and expansion.

411

412

413 **Discussion**

414

415 Neural proliferation zones mediate brain growth, and need to balance NSC maintenance with
416 generation of NPCs and neurons during neurogenesis. Delta/Notch signaling and HES/HER
417 transcription factors play important roles, both in NSC maintenance and control of NPC
418 progression in neurogenesis (Kageyama et al., 2007). HES/HER activities differ during primary
419 neurogenesis in the early neuroepithelium of anamniotes, during embryonic brain growth in neural
420 proliferation zones, and in adult neural stem cell niches (Alunni et al., 2020; Kriegstein and
421 Alvarez-Buylla, 2009). Here, we analyzed Her activities in the zebrafish TPZ, which is highly
422 active in neurogenesis at late embryonic and early larval stages.

423 Among the HES/HER gene families (Chapouton et al., 2011; Zhou et al., 2012) we detected
424 zebrafish homologs of mammalian Hes1, Hes5, and Hes6 expressed in the TPZ. *Hes1* is
425 predominantly regulated by Notch signaling (Hsieh et al., 1997; Jarriault et al., 1995; Jarriault et
426 al., 1998; Nishimura et al., 1998), but also by Notch-independent input (Kageyama et al., 2007;
427 Ohtsuka et al., 1999). In contrast, we find expression of the *Hes1* homologs *her6* and *her9* in the
428 larval NPZs to be largely independent of Notch signaling, in line with previous reports on earlier

429 stages (Bae et al., 2005; Hans et al., 2004; Latimer et al., 2005). *Hes5* expression in mice is Notch-
430 dependent (Ohtsuka et al., 1999). Similarly, for the zebrafish *Hes5* homologs *her4* (Takke et al.,
431 1999; Zhou et al., 2012), *her12* (Gajewski et al., 2006), *her2* and *her15* (Cheng et al., 2015;
432 Shankaran et al., 2007), we find expression to depend on Notch signaling in NPZs. For the zebrafish
433 *Hes6* homologs *her8a*, we find expression in NPZs to depend on Notch signaling, while in the
434 neural plate Notch-independent expression has been reported (Webb et al., 2011). Similarly, *her8.2*
435 appears to be regulated in NPZs by both Notch-dependent and -independent mechanisms.

436 To identify distinct contributions of Notch-dependent and -independent *her* genes to NPZs, we
437 characterized *her* expression and cell type composition of the TPZ in detail (Fig. 11A). At the
438 boundary of thalamus and prethalamus, the ZLI cells (blue) at the ventricular surface express the
439 stem cell marker Sox2, *shh*, and high levels of *her4* and *her15*, as well as low levels of *her9*. In the
440 prethalamus and rostral thalamus, directly adjacent to the ZLI organizer, are Sox2 and, exclusively
441 with respect to *her* genes, *her6* expressing NSCs (green). Within the thalamus, caudal to the *her6*
442 expressing stripe of cells, are Sox2 positive NSCs expressing high levels of *her4* and *her15*, as well
443 as low levels of *her9* (red), similar to the ZLI cells. In the layer of cells directly below the
444 ventricular NSCs, we observed different populations of $Sox2^{low}$ expressing NPCs, expressing low
445 levels of *her4, her15*, and/or *her9* as well as proneural genes: *ascl1a* expression is higher in the
446 rostral prethalamus and rostral thalamus (orange), while *neurog1* expression is higher in a stripe of
447 prethalamic cells adjacent to the ZLI and in the caudal thalamus (yellow). Cells further distal from
448 the ventricular surface are mature neurons, or late progenitors expressing *neurod* family members
449 (grey). Given that TPZ NSCs appear to be characterized by either Notch-dependent or Notch-
450 independent *her* expression, we name the NSCs expressing high *her6* NSCtype1, and those
451 expressing high *her4* and *her15* NSCtype2. The different NSC types emerge during maturation of
452 the thalamic complex, as early *her6* expression comprises the entire presumptive thalamic complex
453 and becomes gradually restricted (Scholpp et al., 2009). The complementary expression of *Hes1*
454 and *Hes5* homologs in zebrafish is consistent with previous findings on *Hes1* and *Hes5* expression
455 in mice (Hatakeyama et al., 2004). However, there are differences: High *Hes1* cells in mice with
456 absent *Ascl1* expression represent quiescent NSCs (Sueda et al., 2019), while NSCtype1 are
457 proliferative. Quiescent versus active NSC populations may not have been established in the larval
458 TPZ, but diversify later in development (Than-Trong et al., 2020).

459 The role of *her4* during neural plate stages was reported to be similar to Notch-dependent
460 *Drosophila E(spl)* genes, as both mediate repression of neurogenesis in the neuroepithelium by
461 lateral inhibition (Nakao and Campos-Ortega, 1996; Takke et al., 1999). We find that in the larval
462 TPZ, *her4* and *her15* continue to depend on Notch signaling and are largely co-expressed. In

463 contrast to the neural plate, where *her4* and *her15* are expressed in domains distinct from *her9*
464 (Stigloher et al., 2008), in the larval TPZ, *her4* and *her15* are co-expressed with *her9*, but expressed
465 in domains distinct from *her6*. A similar dichotomy was observed for the expression of Notch-
466 independent *hairy* versus Notch-dependent *E(spl)* genes in the fruit fly (Fisher and Caudy, 1998;
467 Nakao and Campos-Ortega, 1996).

468 In the zebrafish neural plate, prepatterning genes mark the inter-proneural domains in a Notch-
469 independent manner (Stigloher et al., 2008). For example, *her3* is expressed in two elongated
470 stripes along the anteroposterior axis, flanked by *neurog1* positive progenitor pools (Bae et al.,
471 2000), and *her5* inhibits neurogenesis in the intervening zone at the prospective midbrain-hindbrain
472 boundary (Geling et al., 2004; Ninkovic et al., 2005). These homologs of the *Drosophila hairy*
473 gene appear to act by positioning the proneural domains in the neuroectoderm independent of
474 Notch signaling and are in that respect similar to Drosophila *hairy* function (Fisher and Caudy,
475 1998; Geling et al., 2004). It is therefore tempting to speculate that *her6* and *her9* execute prepattern
476 information to maintain NSCs, and thus might have similar functions as *her3* and *her5* in the neural
477 plate.

478 It was shown that *her6* morphant embryos lose *shha* expression in the mid-diencephalic organizer,
479 which was explained by a premature differentiation of organizer cells accompanied by the loss of
480 the boundary-characteristic *shha* expression (Scholpp et al., 2009). A similar *Shh* phenotype was
481 observed in *Hes1, Hes5* double mutant mice (Baek et al., 2006). In *her6* mutants, we find a severe
482 reduction of *shha* ZLI expression, which is even more severe in *her6, her9* double mutants that
483 lack *shha* expression along the ZLI lateral ventricular walls completely. Despite *her6* and *her9*
484 being expressed in distinct cell populations, *her9* can thus partially compensate *her6* function in
485 the ZLI. Thus, *her6* and *her9* may indeed, in a Notch-independent manner, execute patterning
486 information to maintain ZLI NSCs and signaling activity, similar to *her5* at the zebrafish midbrain-
487 hindbrain boundary (Geling et al., 2004). Analysis of *Hes1* in mice revealed a high expression level
488 mode of *Hes1* function in neural boundaries and organizing centers (Baek et al., 2006), which
489 resulted in a model of two distinct *Hes1* functions. In so-called boundaries, high levels of Hes1
490 constitutively represses neurogenesis, whereas in compartments, its expression oscillates and
491 regulates progression of neurogenesis (Kageyama et al., 2007).

492 Instead of just two in mice, zebrafish have evolved two *Hes1* and nine *Hes5* homologous genes,
493 which appear to differ more strictly in their Notch-dependency. We used a genetic approach to
494 identify differences in Notch-dependent versus -independent *her* gene functions, as well as
495 potential redundancies in the *her* gene network (Fig.11H). Redundancy of *her* genes in zebrafish
496 has been shown for *her1*, *her7* and *her13.2* in somitogenesis (Henry et al., 2002; Oates and Ho,

497 2002; Sieger et al., 2006), as well as for *Hes1* and *Hes5* in mice (Hirata et al., 2001) and *her5* and
498 *her11/him* in zebrafish (Ninkovic et al., 2005) at the mid-hindbrain boundary. However, a detailed
499 analysis of *her* gene interactions and redundancies, as well as a comprehensive understanding of
500 Notch-dependent versus -independent activities has not been obtained.

501 *her6* and *her9* show negative feedback autoregulation and crossregulation, the latter however
502 largely masked in the presence of functional feedback autoregulation, such that the expression of
503 both *her* genes is most strongly upregulated in their double mutants. Due to the cluster deletions,
504 we could not investigate autoregulation of Notch-dependent *her* genes in mutants, however *her4*
505 overexpression reveals negative cross-regulation of *her15.* Overexpression of *her4* did not affect
506 *her6* and *her9* expression*,* confirming that these genes are indeed completely independent of Notch
507 signaling. Overexpression of *her6* repressed *her9, her4* and *her15*, revealing that Notch-
508 independent *her6* activity is in a sense dominant over these *her* genes. Accordingly, *her6* and *her9*
509 expression is largely unaffected in *Df(her4;12)*, *Df(her2;15)* double mutants. We observed
510 alterations in *her4* and *her15* expression in *her6, her9* double mutants, however given that these
511 double mutants affected NSCs composition of the TPZ, the effects at 3 dpf would not necessarily
512 reflect direct regulation. The observed interactions and redundancies are outlined in Fig. 11H.

513 The loss- and gain-of-function experiments also revealed differential contributions of Notch-
514 dependent versus -independent *her* genes to distinct types of NSCs and NPCs in the TPZ. We find
515 that Notch-independent *her6* and *her9* are together critical for a subset of Sox2$^{high}$ NSCs at the
516 lateral ventricular wall of the TPZ, as well as of Sox2$^{low}$ NPCs. This is consistent with an
517 interpretation that Notch-independent *her6* and *her9* activity would be responsible for long-term
518 maintenance of TPZ NSCs, tightly linked to the activity of the ZLI. *her6*, *her9* double mutants also
519 display a TPZ phenotype as well as severe malformations in eye development (data not shown),
520 similar to those reported for *Hes1* mutant mice (Nakamura et al., 2008; Nakamura et al., 2000;
521 Tomita et al., 1996).

522 We were surprised to find that in *Df(her4;12)* or *Df(her2;15)* mutants, as well as in double deficient
523 larvae lacking all 9 zebrafish Notch-dependent *Hes5* homologs, the TPZ appeared morphologically
524 largely normal, and developed an apparently normal NSC and NPC composition of the TPZ (Fig.
525 11D-F). This suggests that in zebrafish, Notch-dependent *her* genes may have only a minor
526 contribution to NSC maintenance. Combined deletion of the eleven zebrafish *Hes1* and *Hes5*
527 homologs in *her*UDMs however, causes loss of most NSCs and essentially all NPCs in the TPZ,
528 resulting in severe morphological malformations of the CNS and retina (Fig. 11G). The *her*UDM
529 phenotype in severity appears similar to the severe *Hes1, Hes5* double mutant phenotype in mice
530 with premature differentiation and stem cell depletion (Baek et al., 2006; Hatakeyama et al., 2004;

531 Ohtsuka et al., 1999). The *her*UDM mutant phenotype is more severe than the *her6, her9* double
532 mutant phenotype, revealing that indeed Notch-dependent *her* genes also contribute to NSC
533 maintenance. Nevertheless, *her6* functions most prominently in this context, as revealed by
534 *her*UDMs rescue by a single WT allele of *her6.* In summary both, Notch-dependent and -
535 independent *her* genes act together to regulate NSC maintenance in the TPZ, with the most
536 prominent activity provided by *her6.*

537 We note that even in the *her*UDMs, proliferating NSCs can be observed at 3 dpf. NSCs in
538 *her*UDMs may be maintained into 3 dpf by additional *her* genes which have their strongest
539 expression early in development, but might still provide some *her* activity to the TPZ, such as *her8a*
540 or *her8.2*, *Hes6* homologs, which we show have both Notch-dependent and -independent aspects
541 of expression in the 2 dpf and at very low levels 3 dpf TPZ.

542 Notch-dependent *Hes/her* genes have been demonstrated to be important regulators of neurogenesis
543 (Nakao and Campos-Ortega, 1996; Takke et al., 1999). Surprisingly, in *Df(her4;12), Df(her2;15)*
544 double deficiency mutants, expression of *ascl1a/b, neurog1* and *olig2* in the TPZ appears largely
545 normal. Thus, in the TPZ, these nine Notch-dependent *her* genes together appear not essential for
546 the initiation of NPCs and proneural gene expression. Our *her4* overexpression experiments
547 support this interpretation: in *her4* heat-shocked embryos, expression of *neurog1* and *neurod1/6b*
548 are largely normal, and of *ascl1b* in most embryos only slightly reduced. In contrast, loss of Notch-
549 independent *her6* and *her9* results in smaller and disorganized domains of *ascl1a/b, neurog1* and
550 *olig2* in the TPZ. Overexpression of *her6* eliminates *neurog1* and *ascl1b* expression, indicating
551 loss of NPCs, and causes a reduction of *neurod1/d6b* expression, revealing reduction of NPCs
552 entering neuronal differentiation. Our findings resemble results in mice, where *Hes5* is upregulated
553 in *Hes1* mutants, but *Hes5* does not regulate *Mash1* (Ishibashi et al., 1995). Similar to our
554 observations with *her6*, *Hes1* single and *Hes1, Hes5* double mutants have much stronger
555 neurogenesis phenotypes than *Hes5* mutants (Hatakeyama et al., 2004).

556 In summary, we were able to show that the expanded number of *Hes1/Hes5* homologous genes in
557 zebrafish goes along with a clear separation of Notch-dependency for different *her* genes, and
558 enables us to differentiate Notch-dependent and -independent *her* activities in NSCs and NPCs.
559 Our genetic analysis demonstrates that the *her* gene network is largely redundant within the Notch-
560 dependent and -independent *her* groups, and that Notch-independent *her* genes may better
561 substitute loss of Notch-dependent genes than vice versa. The observed robustness of the network
562 is supported by several regulatory feedback loops and crossregulation (Fig. 11H). In an intact TPZ,
563 Notch-independent *her* genes predominantly regulate NSC maintenance and NSC transition into
564 the NPC pool, while Notch-dependent *her* genes may predominantly regulate progenitor dynamics

and timing of differentiation, but not progenitor generation itself. This is in line with *Hes5* reported in mice to be responsible for regulation of the transition timing between phases of neurogenesis and gliogenesis, which is accompanied by changes in epigenetic regulation (Bansod et al., 2017). Within the TPZ, we identify two NSC populations: NSCtype1 depends predominantly on Notch-independent *her6* and may interpret patterning information at the ZLI (similar to "boundary" cells by Baek et al., 2006), while NSCtype2 expresses predominantly Notch-dependent *her4* and *her15*. It is tempting to speculate that NSCtype1 may serve long-term NSC maintenance, while NSCtype2 may generate NPCs. How both types, NSCtype2 *her4* and *shha* expressing ZLI organizer cells themselves, and adjacent *her6* expressing NSCtype1, work together to maintain the organizer should help to understand the complexity of the ZLI.

577 # Materials and Methods

578

579 **Zebrafish maintenance and breeding**

580 ABTL strain zebrafish were kept and bred under standard conditions (Westerfield, 2000).
581 Experiments were performed in accordance with the German Animal Welfare Guidelines. All
582 experiments were approved by the ethics committee for animal experiments at the
583 Regierungspräsidium Freiburg.

584 Zebrafish embryos were obtained through natural breeding and embryos were raised in E3 medium
585 (5 mM NaCl, 0.17 mM KCl, 0.33 mM $CaCl_2$, 0.33 mM $MgSO_4$, supplemented with 2 ppm
586 Methylene blue). 0.2 mM N-Phenylthiourea (PTU, Sigma Aldrich) was added to the E3 medium
587 to prevent pigmentation. Embryos were staged as previously described (Kimmel et al., 1995).

588

589 **Embryo fixation and storage**

590 Embryos were incubated in E3 (containing 0.2 mM PTU) supplemented with 1x tricaine
591 methanesulfonate (MS-222) and fixed in 4 % PFA for 4 hours at RT or overnight at 4 °C. Embryos
592 were washed several times with PBST and dehydrated stepwise with 25 %, 50 %, and 75 % MeOH
593 in PBST, and stored at -20 °C in 100 % MeOH.

594

595 **Genotyping**

596 DNA was isolated from embryos or tail biopsies of fixed larvae. Samples were heated 5 min to 95
597 °C in 60 µl TE buffer, after addition of 3 µl Proteinase K (20 mg/ml) digested for at least 4 hrs at
598 55 °C. After heat-inactivation of Proteinase K for 10 min at 95 °C, 3 µl of the DNA sample was
599 used in 30 µl PCR volume. The primer concentration was 0.3 µM unless stated otherwise. PCR
600 programs are supplied in Supplementary Table 3. For genotyping of embryos used in the qPCR, an
601 alkaline lysis was performed. Tails were cut and transferred to 40 µl 50 mM NaOH and incubated
602 for 45 min at 95 °C. The lysis was stopped by addition of 4 µl 1 M Tris-HCl (pH 7.5).

603

604 **Cas9 mRNA and sgRNA generation**

605 Cas9 mRNA was transcribed from the hspCas9 plasmid (Ansai and Kinoshita, 2014) and Cas9-
606 nanos from the Cas9-nanos-3′-UTR plasmid (Moreno-Mateos et al., 2015) using the SP6
607 mMessage mMachine kit (Thermo Fischer), and a polyA tail was added (PolyA tailing kit from

608 Thermo Fischer). sgRNAs were designed with CRISPRscan (Moreno-Mateos et al., 2015) and
609 ordered as oligonucleotides to generate DNA templates (Gagnon et al., 2014). Annealing of the
610 constant oligonucleotide with the variable oligonucleotide was done by cooling from 95 °C down
611 to 25 °C in 1 hr in a PCR machine. Annealed oligonucleotides were filled with T4 DNA Polymerase
612 (New England Biolabs) for 20 min at 11 °C. sgRNAs were transcribed 3-4 hrs at 37 °C using the
613 MEGAscript T7 kit according to protocol (Thermo Fischer) and dissolved in 15 µl $H_2O$.

614

615 **Targeted induction of knockouts and large deficiencies**

616 ***her6 m1358* mutant allele:** Two sgRNAs (transcribed from p3-Oligo04 and p4-Oligo05) were
617 used to generate the *her6* knockout allele *m1358*. The intragenic deletion generates a frameshift
618 that truncates the protein after amino acid 36 before the bHLH domain. Lower case letters are
619 deleted in the mutant allele *m1358*:

620 5'TATAGTGCTTCAAGAagtgattagacagattgactcattttgtttttattttgcattttagtcttctaaacccattatggagaaaaga
621 agaagagcgagaatcaacgaaagcttgggtcagctgaaaacgttaatcttggatgctctgaaaaaagatgtaagtaccgaaagtccgactga
622 gtctttcagttaggctatatctggctggaatattaatgcatttctttatatagccgcatatctaaatcagtctctttcttcactctcagagctccagaca
623 ctctaaacttgagaaagccgacATCCTGGAGATGACA3'

624 ***her9 m1368* mutant allele:** Two sgRNAs (transcribed from p186-Oligo26 and p187-Oligo27)
625 were used to generate the *her9* knockout allele *m1368.* The intragenic deletion generates a
626 frameshift that truncates the protein after amino acid 18 before the bHLH domain. Lower case
627 letters are deleted in the mutant allele *m1368*:

628 5'ATTGCTGGTGCCCCTgccagtggatctcatactcctgacaagccaaagaatgccagcgagcatagaaagtcttcaaagcca
629 atcatggaaaagcgccgcagagcgagaatcaacgagagccttgggcagctgaagactctcattcttgatgctcttaaaaaagatagctccag
630 acactctaaattggagaaagctgatattctggagatgacagtcaagcacctgcgcaatttacaacgtgttcagatgagcgcagccttgtcagct
631 gacacaaacgtcctcagcaagtaccgcgcaggattcaacgagtgcatgaacgaggtgactcgatttctctctacctgcgagggagtgaatac
632 agaggtcagatcgcgacttcttaaccacctgtCCGGTTGTATGGGAC3'

633 ***Df(her2;15) m1490*:** Two sgRNAs (transcribed from p211-Oligo38 and p219-Oligo43) were used
634 to generate the 30 kb deficiency *Df(Chr11:her2,her15.1,her15.2)*, which we abbreviate to
635 *Df(her2;15)* (Fig. S10). 1 nl of the injection mix (6.5 µl total volume), which consisted of 1 µl of
636 each sgRNA (transcribed from Oligo p211 and Oligo p43) plus 4.5 µl Cas9-nanos mRNA (500-
637 800 ng/µl), was injected into 1 cell stage zebrafish embryos. 24 hpf single embryos were genotyped
638 by PCR with two primers p213 + p222 (0.3 µM each) to test for knockout events (Supplementary
639 Table 1). The PCR was performed using MyTaq polymerase (Bioline; PCR program in

640 Supplementary Table 3). If embryos showed the desired deletions, siblings were raised and crossed
641 to ABTL fish. F1 embryos carrying deletions were identified by PCR and siblings were raised to
642 adulthood. Adult F1 fish were fin clipped and genotyped with primers p213 + p222 (0.3 µM each)
643 + p220 (0.08 µM) (Supplementary Tables 1 and 3). Stable heterozygous F2 lines were established
644 and appear to grow normally.

645 ***Df(her4;12) m1364 and m1365*:** Two sgRNAs (transcribed from p39-Oligo12 and p47-Oligo16)
646 were used to generate the 28 kb deficiency *Df(Chr23:her12,her4.1,her4.2,her4.3,her4.4,her4.5)*,
647 which we abbreviate to *Df(her4;12)* (*m1364* and *m1365* are shown in Fig. S10). 1 nl of the injection
648 mix (8.3 µl total volume), which consisted of 1 µl of each sgRNA (transcribed from Oligo12 and
649 Oligo16) plus 6 µl hspCas9 mRNA (600-1200 ng/µl), was injected into 1 cell stage zebrafish
650 embryos. 24 hpf single embryos were genotyped by PCR with p42 + p51 (0.3 µM each) to test for
651 knockout events (Supplementary Table 1). The PCR was performed using MyTaq polymerase
652 (Bioline; PCR program in Supplementary Table 3). If embryos showed deletions, siblings were
653 raised and crossed to ABTL fish. F1 embryos were identified by PCR and siblings were raised to
654 adulthood. Adult F1 fish were fin clipped and genotyped with primers p42 + p43 + p51 (0.3 µM
655 each) (Supplementary Tables 1 and 3). Stable heterozygous F2 lines were established and appear
656 to grow normally.

657 ***her* activity depleted *Df(her2;15), Df(her4;12), her4, her6* (*her*UDM) strain:** The *her9* gene
658 (Chromosome 23: 23,399,520-23,401,305) is only 1.9 Mb away from *her4.5* (Chromosome 23:
659 21,469,203-21,471,022), which is its closest neighbor in the *her4* gene cluster. To obtain the
660 combined *her6*, *her9*, *her4;12* cluster and *her2;15* cluster mutant strain (abbreviated: *her*UDM),
661 *Df(her4;12) m1364* heterozygous embryos were injected with sgRNAs (transcribed from p186-
662 Oligo26 and p187-Oligo27) to target *her9* on the *Df(her4;12)* chromosome. For this mutant, 1 nl
663 of the injection mix (5 µl total volume), which consisted of 1 µl of each sgRNA and 3 µl Cas9-
664 nanos mRNA (500-800 ng/µl), was injected into 1 cell stage zebrafish embryos. The establishment
665 of stable F2 lines was similar as described for the large deficiency mutants. The PCRs were
666 performed with primer p197 and p198 and the program can be found in Supplementary Table 3.
667 The allele was named *her9 m1505.* Lower case letters are deleted in the mutant:

668 5'TGCTGGTGCCCCTGCcagtggatctcatactcctgacaagccaaagaatgccagcgagcatagaaaggtaaaaatcacttat
669 aatgcgattgcatattgttttagaagaatgacagctgcatcagttattctaaaaaaagagagaatgtcttttaattacgtaaattaattaattttccatt
670 tcatctgcagtcttcaaagccaatcatggaaaagcgccgcagagcgagaatcaacgagagccttgggcagctgaagactctcattcttgatg
671 ctcttaaaaaagatgtaagttttatctacaactcttgtcatgcttcagtcacccgacgttagtaattctgaaacagtttctaaccgaattctgctcatt
672 cacagagctccagacactctaaattggagaaagctgatattctggagatgacagtcaagcacctgcgcaatttacaacgtgttcagatgagcg
673 gtaagttgcaagtcagattcctcaagatgataaacttttaacgtgcttttaaaaacgcaatttaatttcctgaatacacaatctaaatacgttttatctt

674 tgtttaccagcagccttgtcagctgacacaaacgtcctcagcaagtaccgcgcaggattcaacgagtgcatgaacgaggtgactcgatttctc
675 tctacctgcgagggagtgaatacagaggtcagatcgcgacttcttaaccacctGTCCGGTTGTATGGG3'

676 When breeding the *her9 m1505, Df(her4;12)* chromosome, we also checked for unwanted crossing
677 over events by PCR for the *Df(her4;12)* allele.

678

679 **LY-411575 treatment**

680 For pharmacological inhibition of Notch signaling by LY-411575 (Rothenaigner et al., 2011),
681 embryos were incubated in E3 supplemented with 0.2 mM PTU until 64 hpf. Then embryos were
682 incubated in 1x E3 supplemented with 0.2 mM PTU, 2 % DMSO, 10 µM LY-411575 for 8 hrs.
683 Control embryos were treated in 1x E3 supplemented with 0.2 mM PTU and 2 % DMSO for 8 hrs
684 in the same six-well plate as the LY treated embryos. Embryos were checked for vital functions
685 and fixed at 72 hpf in 4 % PFA.

686

687 **NICD overexpression**

688 For the overactivation of the Notch signaling pathway, *Tg(hsp:Gal4;UAS:RFP) kca4Tg* were
689 crossed with *Tg(UAS:NICD)kca3Tg* (Scheer and Campos-Ortega, 1999).This allowed heat shock
690 controlled overexpression of NICD. At 64 hpf embryos were heat shocked for 30 min at 40 °C in
691 pre-heated E3 (with 0.2 mM PTU). Heat shocked embryos were then sorted for the heat shock
692 induced RFP marker. Non-fluorescent embryos were used as negative controls. Embryos were
693 tested for the *UAS:NICD* element by PCR (Supplementary Tables 1 and 3).

694

695 **Whole mount immunofluorescence**

696 Fixed and stored embryos were rehydrated with 75 %, 50 %, 25 % MeOH in PBST and washed
697 several times with PBST. Embryos were digested with Proteinase K (10 µg/ml) in PBST for 45
698 min at RT. Embryos were re-fixed with 4 % PFA for 20 min at RT and then washed several times
699 with PBST. Larvae were blocked in blocking solution (1 % BSA, 5 % goat serum, 1 % DMSO in
700 PBST) for 1 hr and incubated with the primary antibodies diluted in blocking solution. The anti-
701 Sox2 antibody ([20G5], abcam, ab171380, LOT GR3253929-5) and the anti-phospho-Histone H3
702 (Ser10) antibody (Merck, #06-570) were diluted 1:400. Embryos were incubated in primary
703 antibodies overnight at 4 °C and then washed several times for 30 min each with PBST
704 supplemented with 1 % DMSO. Embryos were incubated with the secondary antibodies 1:1000 in
705 PBST supplemented with 1 % DMSO and 1 % blocking reagent (Roche, #1096176) overnight at 4

706 °C. Secondary antibodies were Alexa 555 goat anti-mouse IgG (Thermo Fisher Scientific, #A-
707 11001) and Alexa 488 goat anti-rabbit IgG (Thermo Fisher Scientific, #A-11070). Embryos were
708 washed several times in PBST, transferred to 80 % glycerol in PBST and stored at 4°C protected
709 from light. The embryos were recorded soon after staining.

710

711 **RNA detection by Hybridization Chain Reaction (HCR)**

712 Whole mount in situ hybridization by HCR was performed as described in the HCR v3.0 protocol
713 for zebrafish embryo and larvae (Choi et al. (2018) and by Molecular Instruments. The following
714 changes to the protocol were made: In preparation stage 11, 3 dpf larvae were treated with
715 proteinase K (30 µg/ml) for 30 min. In detection stage 1, 15 larvae were used in 2 ml tubes. After
716 amplification stage 6, embryos were washed twice in PBST for 5 min and stored in 80 % glycerol
717 in PBS. Probes for *neurog1* (ENSDART00000078563.5), *asc1a* (ENSDART00000056005.5),
718 *ascl1b* (ENSDART00000183550.1), *sox2* (ENSDART00000104493.5) and *her6*
719 (ENSDART00000023613.9) were ordered and designed by Molecular Instruments.

720 We designed probe sets for *her4* (ENSDART00000079274.4), *her9* (ENSDART00000078936.4),
721 *her15* (ENSDART00000055707.6) and *olig2* (ENSDART00000060006.5) (Supplementary Table
722 2). For example, the *olig2* probe set consists of ten probe pairs which are evenly distributed along
723 the mRNA sequence (Supplementary Table 2). One probe pair consists of two gene specific 25 bp
724 sequences each with a GC content of 37-85 % and a Tm of 55-77 °C. The two sequences were
725 separated by a gap of two nucleotides. The B1 specific spacer and initiator sequences were added
726 to the reverse complement of the two gene specific sequences. The complete probe set was ordered
727 from Sigma Aldrich. Equal volumes of all 20 single probes were mixed and used as probe mixture
728 containing 5 µM of each probe in detection stage 3.

729

730 **Generation of in situ hybridization probes**

731 Specific *her* probes were designed to avoid cross-hybridization of conserved domains. For the
732 generation of *her6*, *her9*, *her4.1-her4.5.*, *her15.1-her15.2*, *her2* and *her12* whole-mount *in situ*
733 hybridizations probes, sequences spanning the last exon and/or 3' UTR of the respective genes
734 were amplified by PCR (all primers for probe generation are given in Supplementary Table 1). The
735 PCRs were performed on WT genomic DNA with PfuUltra II (Agilent). The 50 µl PCR mix
736 contained 6-10 µl dNTP mix (2.5 mM each), 5 µl 10x Pfu buffer, 0.2 mM of each primer, 2 µl
737 DNA and 1 µl PfuUltra II Polymerase. Before cloning, A-overhangs were added by incubating 20
738 µl of the purified PCR product with 9.7 µl MyTaq buffer, 0.2 µl MyTaq polymerase and 0.1 µl (25

739 µM) dATPs for 20 min at 72 °C. After amplification, the probes were cloned into a TOPO vector
740 according to the manufacturer's protocol (TOPO TA cloning kit, Thermo Fisher).

741 For the *her4* probe, which recognizes *her4.1* (ENSDART00000079274.4), *her4.2*
742 (ENSDART00000137573.2), *her4.3* (ENSDART00000104209.4), *her4.4*
743 ENSDART00000079265.6) and *her4.5* (ENSDART00000104206.4), a template was generated
744 with primer p159F and p160R (annealing 57 °C, 40 sec). For the *her15* probe, which recognizes
745 *her15.1* (ENSDART00000055707.6) and *her15.2* (ENSDART00000055706.6), a template was
746 cloned using primers p157F and p158F (annealing 56 °C, 40 sec). The *her2*
747 (ENSDART00000055709.5) probe template was amplified with p154F and p155R (annealing 56
748 °C, 40 sec) and the *her12* (ENSDART00000044080.7) probe template was amplified with p152F
749 and p153R (annealing 56 °C, 40 sec). The *her6* (ENSDART00000023613.9) probe template was
750 amplified using p147F and p148R (annealing 57 °C, 55 sec) and the *her9*
751 (ENSDART00000078936.4) probe template was amplified with p149F and p150R (annealing 56
752 °C 40 sec). All primers are given in Supplementary Table1.

753 The *her8a* (ENSDART00000123395.4) probe template was amplified as published in Webb et al.
754 (2011) with p322F and p327R (annealing 56 °C, 1 min) and the *her8.2*
755 (ENSDART00000101578.4) probe template was amplified with p260F and p259R (annealing 56
756 °C, 1 min). For *her8a* and *her8.2* cDNA was used as a template in the PCR.

757 *sox2* (ENSDART00000104493.5), *neurod1* (ENSDART00000011837.6), *neurog1*
758 (ENSDART00000078563.5), *shha* (ENSDART00000149395.3), *neurod6b*
759 (ENSDART00000185805.1), *irx1b* (ENSDART00000079114.6; (Scholpp et al., 2009), *ascl1a*
760 (ENSDART00000056005.5; Allende and Weinberg (1994), *ascl1b* (ENSDART00000183550.1;
761 Allende and Weinberg (1994) probes have been previously published (www.zfin.org) and plasmids
762 were validated by sequencing.

763 Plasmids were linearized and transcribed with T7 or SP6 RNA Polymerases (Thermo Fischer).
764 Antisense RNA probes were generated using the DIG or DNP based RNA labelling kits from Roche
765 (Merck, Germany). The quality of the RNA probe was checked by agarose gel electrophoresis.

766

767 **Whole-mount in situ hybridizations**

768 Chromogenic whole mount in situ hybridizations were performed as previously described
769 (Holzschuh et al., 2003). After fixation, storage and rehydration, embryos were washed three times
770 in PBST and treated with 10 µg/ml Proteinase K (AppliChem, 15 min incubation per 24 hrs of
771 development). Embryos were washed with PBST and fixed in 4% PFA for 20 min at room

772 temperature. Embryos were washed 5 times in PBST and incubated in hybridization mix (50%
773 formamide, 5x SSC, 5 mg/ml torula yeast RNA type IV, 50 µg/ml heparin, 0.1% Tween-20) at 65
774 °C for 4 hrs. Next, embryos were incubated with digoxigenin labelled antisense RNA probes in
775 hybridization mix (dilution 1:200 - 1:500) at 65 °C overnight. After hybridization, embryos were
776 washed at 65 °C for 20 min each with the following solutions: twice with 50% formamide in 2x
777 SSCT, twice with 25% formamide in 2x SSCT for 20 min each, twice in 2x SSCT for 20 min each,
778 three times in 0.2x SSCT for 20 min each. Next, embryos were washed once in 0.1x SSCT in 0.5x
779 PBST for 10 min and twice in PBST for 10 min each at room temperature. Embryos were blocked
780 for 2 to 3 hrs with 2 % heat inactivated goat serum (Vector Laboratories) and 4 mg/ml BSA
781 (AppliChem) in PBST. Embryos were incubated overnight at 4 °C in blocking solution
782 supplemented with the alkaline phosphatase coupled anti-digoxigenin antibody (Roche, REF
783 11093274910) 1:3000. Embryos were washed six times in PBST at room temperature for 20 min
784 each and three times in NTMT (100 mM NaCl, 100 mM Tris-HCl at pH 9.5, 50 mM $MgCl_2$, 0.1 %
785 Tween-20) for 15 min each. For the staining reaction, 0.18 mg/ml BCIP (5-bromo-4-chloro-3-
786 indolyl-phosphate, AppliChem) and 0.45 mg/ml NBT (4-nitroblue tetrazolium chloride,
787 AppliChem) were added to NTMT. Staining was performed in the dark and stopped by 3 washes
788 in PBST supplemented with 0.1 mM EDTA. For longer storage, embryos were fixed in 4 % PFA
789 for 1 hr at room temperature. After three more washes in PBST, embryos were transferred to 80%
790 glycerol in PBST supplemented with 0.1 mM EDTA and stored at 4 °C protected from light.

791

792 **Fluorescent whole-mount in situ hybridizations**

793 Fluorescent in situ hybridizations were performed as described in the section whole mount in situ
794 hybridization until addition of probes. The digoxigenin and dinitrophenol labelled antisense probes
795 (see "Generation of in situ hybridization probes") together were added to the hybridization mix and
796 the embryos were incubated at 65 °C overnight. Washes were performed at 65 °C as described
797 above. Embryos were washed in TNT (100 mM Tris-HCl at pH 7.5, 150 mM NaCl, 0.5 % Tween-
798 20) and blocked in TNT supplemented with 1 % Boehringer Block (Roche) for 2 to 3 hrs at room
799 temperature. The anti-digoxigenin-POD Fab fragment antibody (Roche, REF 11207733910) was
800 used 1:400 in blocking solution and embryos were incubated overnight at 4 °C. Embryos were
801 washed eight times 15 min each in TNT at room temperature, rinsed in 100 mM borate buffer pH
802 8.0 and incubated in staining mix containing 2 % dextrane sulfate, 1% tyramide stock solution
803 Alexa Fluor 488 (Thermo Fischer), 0.0015 % $H_2O_2$ and 112.5 µg/ml 4-iodphenole in 100 mM
804 borate buffer pH 8.0 for 1 hr at room temperature. Embryos were washed three times in TNT,
805 incubated in 0.3 % $H_2O_2$ in TNT for 30 min and then washed five times in TNT for five minutes

806 each at room temperature. Embryos were blocked in 1% blocking reagent (Roche) in 100 mM
807 maleic acid, 150 mM NaCl at pH 7.5 for 2 to 3 hrs at room temperature. The anti-DNP HRP
808 antibody (Perkin Elmer, FP1129) was used 1:200 in blocking solution and embryos were incubated
809 overnight at 4 °C. Embryos were washed eight times 15 min each in TNT at room temperature,
810 rinsed in 100 mM borate buffer pH 8.0 and incubated in staining mix containing 2 % dextrane
811 sulfate, 1 % tyramide stock solution Alexa Fluor 555 (Thermo Fischer), 0.0015 % $H_2O_2$ and 112.5
812 µg/ml 4-iodphenole in 100 mM borate buffer pH 8.0 for 1 hr at room temperature. Embryos were
813 washed three times in TNT and three times in PBST for five minutes each at room temperature.
814 Embryos were transferred to 80 % glycerol in PBS and stored at 4 °C protected from light.

815

816 **Microscopy**

817 Imaging of chromogenic whole mount in situ hybridizations was performed with the Zeiss
818 Axioskop2, Axiovision SE64, Rel.4.9.1 with AxioCam ICc1 with a Plan-Neofluar 20×/0.5 or
819 10×/0.3 objective and DIC optics. Embryos were mounted in 80 % glycerol in PBST supplemented
820 with 0.1 mM EDTA or in 80 % glycerol in $H_2O$ supplemented with 1 % standard agarose (Bioron).
821 All shown images are single z-planes from an image stack.

822 Imaging of fluorescent stainings was performed with an inverted microscope with LSM-880
823 Airyscan (Zeiss). A 40x objective LD LCI Plan Apochromat 40x/1.2 autocorr (Zeiss) was used.
824 Embryos were embedded in 80% glycerol in $H_2O$ supplemented with 1 % standard agarose
825 (Bioron). The immersion medium was glycerol. The imaging program ZEN 2.3 SP1 FP3 (black)
826 version 14.0.22.201 was used. If Airyscan was used, image stacks were processed with the ZEN
827 black software using the Airyscan algorithm (v. 2.3 SP1 Zeiss). All images shown are single z-
828 planes from an image stack, except for Fig. 2A,B,C; Fig. 4A,B,C,C'', D, D''; Fig. 7A,B,C,C'',D,
829 D'', Fig. 10C,D, E,F and Fig. S3A,B, which show orthogonal projections of an image stack. Fig.
830 2D, D' and D'' show single z planes from an image stack of laterally mounted embryos.

831 Figures were assembled in Photoshop. Image levels were linearly adjusted except for Fig. 5B-C',
832 F-G', Fig. S8 and Fig. S9A-F' to improve visibility in very dark stained areas.

833

834 **Numbers of embryos analyzed**

835 For WISH experiments analyzing WT, compound treated or heat shock overexpression treated
836 embryos, shown in Fig. 1G-R', Fig 8, Fig. 9, Fig. S1, Fig. S2 G-J' and Fig. S11, for each condition
837 10-20 larvae were examined for their expression patterns and representative images are shown.

838 When the (n) numbers are provided in images or legends, the number indicates how many larvae
839 were imaged. If staining patterns or intensity varied within one experimental condition (Fig. 9B',
840 E' and J'), one embryo with a staining pattern representative for the majority of embryos analyzed
841 is shown, and the numbers in the bottom right corner indicate the number of embryos with the
842 representative expression pattern and the total number of embryos analyzed for this condition.

843 For analysis of genetic mutants or fluorescent WISH shown in Fig. 1A-F', Fig. 2, Fig. 3C-N', Fig
844 4, Fig. 5, Fig. 6C-F', Fig. 7, Fig. 10, Fig.S2A-D', Fig. S3, Fig. S8, Fig. S9, the numbers (n) of
845 embryos imaged for each condition are provided in the Figure legends or in the image panels, and
846 in Supplementary Table 4.

847

848 **qPCR**

849 The tail of each 4 dpf larva was cut and transferred to a new tube for genotyping as described above.
850 The rest of each larva was stored individually in 75 µl RNA later solution (Ambion, AM7024) on
851 ice. Following genotype detection by PCR, total RNA was extracted from 2-3 embryos pooled per
852 genotype using the RNeasy Mini Kit (QIAGEN, 74106) and QIAshredder columns (QIAGEN,
853 79656). The sample was homogenized in 1 % β-mercaptoethanol in 600 µl RLT buffer
854 (QUIAGEN, 74106). The suspension was transferred to a QIAshredder column and centrifuged for
855 1 min at 10,000 g. 700 µl 70 % ethanol was added to the flow through and transferred to RNeasy
856 Mini spin columns. After centrifugation (15 s, 10,000 g), 350 µl RW1 buffer (QUIAGEN, 74106)
857 was added to the membrane and centrifuged. A digestion step with DNase I was performed by
858 adding 80 µl of the DNase I incubation mix (consisting of 10 µl DNase I stock solution with a
859 concentration of 2.73 Kunitz units/µl and 70µl RDD buffer; QUIAGEN, 74106) to the RNeasy
860 spin column membrane for 15 min on the benchtop to remove DNA from the membrane. After two
861 more washing steps according to manufacturer's protocol, the column was dried by centrifugation
862 for additional 2 min. Total RNA was eluted by adding 30 µl $H_2O$ to the filter membrane. Tubes
863 were incubated for 1 min at RT and centrifuged for 1 min at 10,000 g. The RNA concentrations
864 were determined by NanoDrop measurements.

865 100 ng total RNA was used as a template for reverse transcription into cDNA. cDNA was generated
866 with the SuperScript III RT Kit according to manufacturer's protocol using oligo$(dT)_{12-18}$ (0.5
867 µg/µl) primers. The qPCR was performed with the SYBR Green Supermix (Sso Advanced
868 Universal, Biorad). The 10 µl qPCR mix contained 5 µl 2x SYBR Green Supermix, 1 µl primer
869 mix (0.5 µM final concentration of each primer) and 2 µl cDNA. The PCR plate was carefully
870 sealed and centrifuged for 10 min at 3000 rpm. qPCRs were performed with the LightCycler

871 (Roche) and programs are given in Supplementary Table 3. The data analysis was performed as in
872 Taylor et al. (2019), and *actb2* was used as reference gene. We note that for calculations of relative
873 expression, we excluded one of the three biological replicates for the double mutant since the CT
874 value for *actb2* control in this replicate was off. Therefore, the number of biological replicates for
875 *her6* and *her9* qPCR in *her6, her9* double mutants is two. For all others the number of biological
876 replicates is three.

877

878

879 ## References (including references in methods)


880 **Adolf, B., Chapouton, P., Lam, C. S., Topp, S., Tannhauser, B., Strahle, U., Götz, M. and**
881 **Bally-Cuif, L.** (2006). Conserved and acquired features of adult neurogenesis in the
882 zebrafish telencephalon. *Dev Biol* **295**, 278-293.

883 **Allende, M. L. and Weinberg, E. S.** (1994). The expression pattern of two zebrafish achaete-
884 scute homolog (ash) genes is altered in the embryonic brain of the cyclops mutant. *Dev*
885 *Biol* **166**, 509-530.

886 **Alunni, A., Coolen, M., Foucher, I. and Bally-Cuif, L.** (2020). Neurogenesis in zebrafish. In
887 *Patterning and Cell Type Specification in the Developing CNS and PNS* (ed. J.
888 Rubenstein, P. Rakic, B. Chen & K. Y. Kwan), pp. 643-697: Academic Press.

889 **Ansai, S. and Kinoshita, M.** (2014). Targeted mutagenesis using CRISPR/Cas system in
890 medaka. *Biol Open* **3**, 362-371.

891 **Bae, S., Bessho, Y., Hojo, M. and Kageyama, R.** (2000). The bHLH gene Hes6, an inhibitor of
892 Hes1, promotes neuronal differentiation. *Development* **127**, 2933-2943.

893 **Bae, Y. K., Shimizu, T. and Hibi, M.** (2005). Patterning of proneuronal and inter-proneuronal
894 domains by hairy- and enhancer of split-related genes in zebrafish neuroectoderm.
895 *Development* **132**, 1375-1385.

896 **Baek, J. H., Hatakeyama, J., Sakamoto, S., Ohtsuka, T. and Kageyama, R.** (2006). Persistent
897 and high levels of Hes1 expression regulate boundary formation in the developing central
898 nervous system. *Development* **133**, 2467-2476.

899 **Bansod, S., Kageyama, R. and Ohtsuka, T.** (2017). Hes5 regulates the transition timing of
900 neurogenesis and gliogenesis in mammalian neocortical development. *Development* **144**,
901 3156-3167.

902 **Chapouton, P., Webb, K. J., Stigloher, C., Alunni, A., Adolf, B., Hesl, B., Topp, S.,**
903 **Kremmer, E. and Bally-Cuif, L.** (2011). Expression of hairy/enhancer of split genes in
904 neural progenitors and neurogenesis domains of the adult zebrafish brain. *J Comp Neurol*
905 **519**, 1748-1769.

906 **Cheng, Y. C., Chiang, M. C., Shih, H. Y., Ma, T. L., Yeh, T. H., Huang, Y. C., Lin, C. Y.**
907 **and Lin, S. J.** (2015). The transcription factor hairy/E(spl)-related 2 induces proliferation
908 of neural progenitors and regulates neurogenesis and gliogenesis. *Dev Biol* **397**, 116-128.

909 **Choi, H. M. T., Schwarzkopf, M., Fornace, M. E., Acharya, A., Artavanis, G., Stegmaier, J.,**
910 **Cunha, A. and Pierce, N. A.** (2018). Third-generation in situ hybridization chain
911 reaction: multiplexed, quantitative, sensitive, versatile, robust. *Development* **145**.

912 **Davis, R. L. and Turner, D. L.** (2001). Vertebrate hairy and Enhancer of split related proteins:
913 transcriptional repressors regulating cellular differentiation and embryonic patterning.
914 *Oncogene* **20**, 8342-8357.

915 **Fisher, A. and Caudy, M.** (1998). The function of hairy-related bHLH repressor proteins in cell
916 fate decisions. *Bioessays* **20**, 298-306.

917 **Gagnon, J. A., Valen, E., Thyme, S. B., Huang, P., Akhmetova, L., Pauli, A., Montague, T.**
918 **G., Zimmerman, S., Richter, C. and Schier, A. F.** (2014). Efficient mutagenesis by
919 Cas9 protein-mediated oligonucleotide insertion and large-scale assessment of single-
920 guide RNAs. *PLoS One* **9**, e98186.

921 **Gajewski, M., Elmasri, H., Girschick, M., Sieger, D. and Winkler, C.** (2006). Comparative
922 analysis of her genes during fish somitogenesis suggests a mouse/chick-like mode of
923 oscillation in medaka. *Dev Genes Evol* **216**, 315-332.

924 **Geling, A., Plessy, C., Rastegar, S., Strahle, U. and Bally-Cuif, L.** (2004). Her5 acts as a
925 prepattern factor that blocks *neurogenin1* and *coe2* expression upstream of Notch to
926 inhibit neurogenesis at the midbrain-hindbrain boundary. *Development* **131**, 1993-2006.

927 **Grandel, H., Kaslin, J., Ganz, J., Wenzel, I. and Brand, M.** (2006). Neural stem cells and
928 neurogenesis in the adult zebrafish brain: origin, proliferation dynamics, migration and
929 cell fate. *Dev Biol* **295**, 263-277.

930 **Hans, S., Scheer, N., Riedl, I., v Weizsacker, E., Blader, P. and Campos-Ortega, J. A.**
931 (2004). her3, a zebrafish member of the hairy-E(spl) family, is repressed by Notch
932 signalling. *Development* **131**, 2957-2969.

933 **Hatakeyama, J., Bessho, Y., Katoh, K., Ookawara, S., Fujioka, M., Guillemot, F. and**
934 **Kageyama, R.** (2004). Hes genes regulate size, shape and histogenesis of the nervous
935 system by control of the timing of neural stem cell differentiation. *Development* **131**,
936 5539-5550.

937 **Henry, C. A., Urban, M. K., Dill, K. K., Merlie, J. P., Page, M. F., Kimmel, C. B. and**
938 **Amacher, S. L.** (2002). Two linked hairy/Enhancer of split-related zebrafish genes, her1
939 and her7, function together to refine alternating somite boundaries. *Development* **129**,
940 3693-3704.

941 **Hirata, H., Tomita, K., Bessho, Y. and Kageyama, R.** (2001). Hes1 and Hes3 regulate
942 maintenance of the isthmic organizer and development of the mid/hindbrain. *EMBO J* **20**,
943 4454-4466.

944 **Holzschuh, J., Hauptmann, G. and Driever, W.** (2003). Genetic analysis of the roles of Hh,
945 FGF8, and nodal signaling during catecholaminergic system development in the zebrafish
946 brain. *J Neurosci* **23**, 5507-5519.

947 **Hsieh, J. J., Nofziger, D. E., Weinmaster, G. and Hayward, S. D.** (1997). Epstein-Barr virus
948 immortalization: Notch2 interacts with CBF1 and blocks differentiation. *J Virol* **71**, 1938-
949 1945.

950 **Imayoshi, I., Isomura, A., Harima, Y., Kawaguchi, K., Kori, H., Miyachi, H., Fujiwara, T.,**
951 **Ishidate, F. and Kageyama, R.** (2013). Oscillatory control of factors determining
952 multipotency and fate in mouse neural progenitors. *Science* **342**, 1203-1208.

953 **Ishibashi, M., Ang, S. L., Shiota, K., Nakanishi, S., Kageyama, R. and Guillemot, F.** (1995).
954 Targeted disruption of mammalian hairy and Enhancer of split homolog-1 (HES-1) leads
955 to up-regulation of neural helix-loop-helix factors, premature neurogenesis, and severe
956 neural tube defects. *Genes Dev* **9**, 3136-3148.

957 **Ishibashi, M., Moriyoshi, K., Sasai, Y., Shiota, K., Nakanishi, S. and Kageyama, R.** (1994).
958 Persistent expression of helix-loop-helix factor HES-1 prevents mammalian neural
959 differentiation in the central nervous system. *EMBO J* **13**, 1799-1805.

960 **Itoh, M., Kim, C. H., Palardy, G., Oda, T., Jiang, Y. J., Maust, D., Yeo, S. Y., Lorick, K.,**
961 **Wright, G. J., Ariza-McNaughton, L., et al.** (2003). Mind bomb is a ubiquitin ligase
962 that is essential for efficient activation of Notch signaling by Delta. *Dev Cell* **4**, 67-82.

963 **Jarriault, S., Brou, C., Logeat, F., Schroeter, E. H., Kopan, R. and Israel, A.** (1995).
964 Signalling downstream of activated mammalian Notch. *Nature* **377**, 355-358.

965 **Jarriault, S., Le Bail, O., Hirsinger, E., Pourquie, O., Logeat, F., Strong, C. F., Brou, C.,**
966 **Seidah, N. G. and Isra l, A.** (1998). Delta-1 activation of notch-1 signaling results in
967 HES-1 transactivation. *Mol Cell Biol* **18**, 7423-7431.

968 **Jennings, B., Preiss, A., Delidakis, C. and Bray, S.** (1994). The Notch signalling pathway is
969 required for Enhancer of split bHLH protein expression during neurogenesis in the
970 Drosophila embryo. *Development* **120**, 3537-3548.

971 **Kageyama, R., Ohtsuka, T. and Kobayashi, T.** (2007). The Hes gene family: repressors and
972 oscillators that orchestrate embryogenesis. *Development* **134**, 1243-1251.

**Kimmel, C. B., Ballard, W. W., Kimmel, S. R., Ullmann, B. and Schilling, T. F.** (1995). Stages of embryonic development of the zebrafish. *Dev Dyn* **203**, 253-310.

**Kishimoto, N., Shimizu, K. and Sawamoto, K.** (2012). Neuronal regeneration in a zebrafish model of adult brain injury. *Dis Model Mech* **5**, 200-209.

**Koyano-Nakagawa, N., Kim, J., Anderson, D. and Kintner, C.** (2000). Hes6 acts in a positive feedback loop with the neurogenins to promote neuronal differentiation. *Development* **127**, 4203-4216.

**Kriegstein, A. and Alvarez-Buylla, A.** (2009). The glial nature of embryonic and adult neural stem cells. *Annu Rev Neurosci* **32**, 149-184.

**Latimer, A. J., Shin, J. and Appel, B.** (2005). her9 promotes floor plate development in zebrafish. *Dev Dyn* **232**, 1098-1104.

**Moreno-Mateos, M. A., Vejnar, C. E., Beaudoin, J. D., Fernandez, J. P., Mis, E. K., Khokha, M. K. and Giraldez, A. J.** (2015). CRISPRscan: designing highly efficient sgRNAs for CRISPR-Cas9 targeting in vivo. *Nat Methods* **12**, 982-988.

**Mueller, T.** (2012). What is the Thalamus in Zebrafish? *Front Neurosci* **6**, 64.

**Mueller, T. and Wullimann, M. F.** (2016). Atlas of Early Zebrafish Brain Development. *Amsterdam: Elsevier Academic Press.*

**Nakamura, T., Ohtsuka, T., Sekiyama, E., Cooper, L. J., Kokubu, H., Fullwood, N. J., Barrandon, Y., Kageyama, R. and Kinoshita, S.** (2008). Hes1 regulates corneal development and the function of corneal epithelial stem/progenitor cells. *Stem Cells* **26**, 1265-1274.

**Nakamura, Y., Sakakibara, S., Miyata, T., Ogawa, M., Shimazaki, T., Weiss, S., Kageyama, R. and Okano, H.** (2000). The bHLH gene Hes1 as a repressor of the neuronal commitment of CNS stem cells. *Journal of Neuroscience* **20**, 283-293.

**Nakao, K. and Campos-Ortega, J. A.** (1996). Persistent expression of genes of the enhancer of split complex suppresses neural development in Drosophila. *Neuron* **16**, 275-286.

**Ninkovic, J., Tallafuss, A., Leucht, C., Topczewski, J., Tannhauser, B., Solnica-Krezel, L. and Bally-Cuif, L.** (2005). Inhibition of neurogenesis at the zebrafish midbrain-hindbrain boundary by the combined and dose-dependent activity of a new hairy/E(spl) gene pair. *Development* **132**, 75-88.

**Nishimura, M., Isaka, F., Ishibashi, M., Tomita, K., Tsuda, H., Nakanishi, S. and Kageyama, R.** (1998). Structure, chromosomal locus, and promoter of mouse Hes2 gene, a homologue of Drosophila hairy and Enhancer of split. *Genomics* **49**, 69-75.

**Oates, A. C. and Ho, R. K.** (2002). Hairy/E(spl)-related (Her) genes are central components of the segmentation oscillator and display redundancy with the Delta/Notch signaling pathway in the formation of anterior segmental boundaries in the zebrafish. *Development* **129**, 2929-2946.

**Ohtsuka, T., Ishibashi, M., Gradwohl, G., Nakanishi, S., Guillemot, F. and Kageyama, R.** (1999). Hes1 and Hes5 as notch effectors in mammalian neuronal differentiation. *EMBO J* **18**, 2196-2207.

**Onichtchouk, D., Geier, F., Polok, B., Messerschmidt, D. M., Mossner, R., Wendik, B., Song, S., Taylor, V., Timmer, J. and Driever, W.** (2010). Zebrafish Pou5f1-dependent transcriptional networks in temporal control of early development. *Mol Syst Biol* **6**, 354.

**Pasini, A., Jiang, Y. J. and Wilkinson, D. G.** (2004). Two zebrafish Notch-dependent hairy/Enhancer-of-split-related genes, her6 and her4, are required to maintain the coordination of cyclic gene expression in the presomitic mesoderm. *Development* **131**, 1529-1541.

1020 **Riddihough, G. and Ish-Horowicz, D.** (1991). Individual stripe regulatory elements in the
1021 Drosophila hairy promoter respond to maternal, gap, and pair-rule genes. *Genes Dev* **5**,
1022 840-854.

1023 **Rothenaigner, I., Krecsmarik, M., Hayes, J. A., Bahn, B., Lepier, A., Fortin, G., Gotz, M.,**
1024 **Jagasia, R. and Bally-Cuif, L.** (2011). Clonal analysis by distinct viral vectors identifies
1025 bona fide neural stem cells in the adult zebrafish telencephalon and characterizes their
1026 division properties and fate. *Development* **138**, 1459-1469.

1027 **Sasai, Y., Kageyama, R., Tagawa, Y., Shigemoto, R. and Nakanishi, S.** (1992). Two
1028 mammalian helix-loop-helix factors structurally related to Drosophila hairy and Enhancer
1029 of split. *Genes Dev* **6**, 2620-2634.

1030 **Scheer, N. and Campos-Ortega, J. A.** (1999). Use of the Gal4-UAS technique for targeted gene
1031 expression in the zebrafish. *Mech Dev* **80**, 153-158.

1032 **Scholpp, S., Delogu, A., Gilthorpe, J., Peukert, D., Schindler, S. and Lumsden, A.** (2009).
1033 Her6 regulates the neurogenetic gradient and neuronal identity in the thalamus. *Proc Natl*
1034 *Acad Sci U S A* **106**, 19895-19900.

1035 **Scholpp, S. and Lumsden, A.** (2010). Building a bridal chamber: development of the thalamus.
1036 *Trends Neurosci* **33**, 373-380.

1037 **Scholpp, S., Wolf, O., Brand, M. and Lumsden, A.** (2006). Hedgehog signalling from the zona
1038 limitans intrathalamica orchestrates patterning of the zebrafish diencephalon.
1039 *Development* **133**, 855-864.

1040 **Shankaran, S. S., Sieger, D., Schroter, C., Czepe, C., Pauly, M. C., Laplante, M. A., Becker,**
1041 **T. S., Oates, A. C. and Gajewski, M.** (2007). Completing the set of h/E(spl) cyclic genes
1042 in zebrafish: her12 and her15 reveal novel modes of expression and contribute to the
1043 segmentation clock. *Dev Biol* **304**, 615-632.

1044 **Sieger, D., Ackermann, B., Winkler, C., Tautz, D. and Gajewski, M.** (2006). her1 and her13.2
1045 are jointly required for somitic border specification along the entire axis of the fish
1046 embryo. *Dev Biol* **293**, 242-251.

1047 **Sieger, D., Tautz, D. and Gajewski, M.** (2004). her11 is involved in the somitogenesis clock in
1048 zebrafish. *Dev Genes Evol* **214**, 393-406.

1049 **Stigloher, C., Chapouton, P., Adolf, B. and Bally-Cuif, L.** (2008). Identification of neural
1050 progenitor pools by E(Spl) factors in the embryonic and adult brain. *Brain Res Bull* **75**,
1051 266-273.

1052 **Sueda, R., Imayoshi, I., Harima, Y. and Kageyama, R.** (2019). High Hes1 expression and
1053 resultant Ascl1 suppression regulate quiescent vs. active neural stem cells in the adult
1054 mouse brain. *Genes Dev* **33**, 511-523.

1055 **Takke, C., Dornseifer, P., Von Weizsacker, E. and Campos-Ortega, J. A.** (1999). her4, a
1056 zebrafish homologue of the Drosophila neurogenic gene E(spl), is a target of NOTCH
1057 signalling. *Development* **126**, 1811-1821.

1058 **Taylor, S. C., Nadeau, K., Abbasi, M., Lachance, C., Nguyen, M. and Fenrich, J.** (2019). The
1059 Ultimate qPCR Experiment: Producing Publication Quality, Reproducible Data the First
1060 Time. *Trends Biotechnol* **37**, 761-774.

1061 **Than-Trong, E., Kiani, B., Dray, N., Ortica, S., Simons, B., Rulands, S., Alunni, A. and**
1062 **Bally-Cuif, L.** (2020). Lineage hierarchies and stochasticity ensure the long-term
1063 maintenance of adult neural stem cells. *Sci Adv* **6**, eaaz5424.

1064 **Tomita, K., Ishibashi, M., Nakahara, K., Ang, S. L., Nakanishi, S., Guillemot, F. and**
1065 **Kageyama, R.** (1996). Mammalian hairy and Enhancer of split homolog 1 regulates
1066 differentiation of retinal neurons and is essential for eye morphogenesis. *Neuron* **16**, 723-
1067 734.

1068 **Virolainen, S. M., Achim, K., Peltopuro, P., Salminen, M. and Partanen, J.** (2012).
1069 Transcriptional regulatory mechanisms underlying the GABAergic neuron fate in
1070 different diencephalic prosomeres. *Development* **139**, 3795-3805.

1071 **Webb, K. J., Coolen, M., Gloeckner, C. J., Stigloher, C., Bahn, B., Topp, S., Ueffing, M. and**
1072 **Bally-Cuif, L.** (2011). The Enhancer of split transcription factor Her8a is a novel
1073 dimerisation partner for Her3 that controls anterior hindbrain neurogenesis in zebrafish.
1074 *BMC Dev Biol* **11**, 27.

1075 **Westerfield, M.** (2000). *The zebrafish book. A guide for the laboratory use of zebrafish (Danio*
1076 *rerio)* (4th edn). Eugene, USA: Univ. of Oregon Press.

1077 **Zhou, M., Yan, J., Ma, Z., Zhou, Y., Abbood, N. N., Liu, J., Su, L., Jia, H. and Guo, A. Y.**
1078 (2012). Comparative and evolutionary analysis of the HES/HEY gene family reveal
1079 exon/intron loss and teleost specific duplication events. *PLoS One* **7**, e40649.

1080 **Zupanc, G. K.** (2001). Adult neurogenesis and neuronal regeneration in the central nervous
1081 system of teleost fish. *Brain Behav Evol* **58**, 250-275.

1082 **Zupanc, G. K., Hinsch, K. and Gage, F. H.** (2005). Proliferation, migration, neuronal
1083 differentiation, and long-term survival of new cells in the adult zebrafish brain. *J Comp*
1084 *Neurol* **488**, 290-319.

1085

1086

**Acknowledgements**

We thank Sylke Lange for technical assistance, the Life Imaging Center (LIC) for support in confocal imaging and image analysis, and Sabine Götter for excellent fish care. We thank Beatrice Weber for initial characterization of *her4* and *her6* mutant embryos, Masha Miranda Tolentino Voigt for initial characterization Notch-dependency of *her* genes, Samuel Wöhrle for initial characterization of *Tg(hsp:her6-FLAG*) embryos, Leonie Bohnert for establishing the HCR-RNA FISH technique in our lab, and Niklas Mayle for performing the WISH procedure for *shha* expression in *her6* and *her9* mutants. We thank Christian Altbürger for scientific discussion. The *neurod1* and *neurog1* plasmids were obtained from Patrick Blader. We thank Chaitanya Dingare for advice on designing the *olig2* HCR probe, and Rebecca Peters for help in designing Fig. 11H.

**Competing interests**

The authors declare no competing or financial interests.

**Ethics Oversight**: All animal experiments were approved by state authorities (Regierungspraesidium Freiburg permits 35-9185/G-16/123, 35-9185.81/G-19/19 and 35-9185.81/G-19/54).

**Data availability**

All primary image data are available on request.

**Funding**

This work was funded by grants from the Deutsche Forschungsgemeinschaft (DFG, German Research Foundation) under Germany´s Excellence Strategy – EXC-2189 CIBSS– Project ID: 390939984 (Gefördert durch die Deutsche Forschungsgemeinschaft (DFG) im Rahmen der Exzellenzstrategie des Bundes und der Länder – EXC-2189 – Projektnummer 390939984), the Excellence Initiative of the German Federal and State Governments (BIOSS - EXC 294), and CRC 850.

**Supplementary information**

Supplementary Figures S1-S11 (one PDF file)

Supplementary Data Tables S1-S5 (one PDF file)

Supplementary Movies S1-S5 (separate mp4 files)

## Main Figures

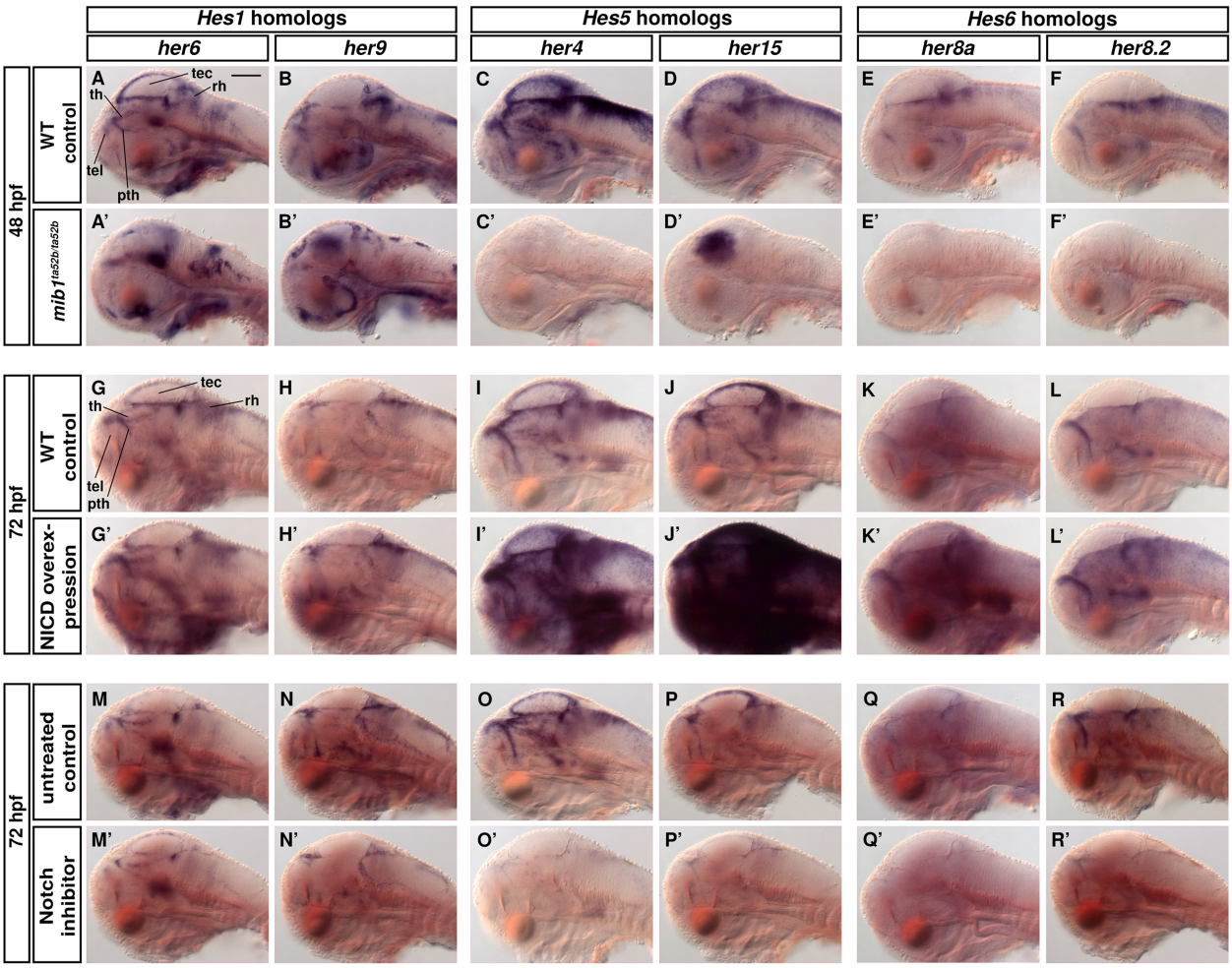


**Fig. 1 Notch signaling dependent and independent *her* gene expression**

**(A-R')** *her6, her9, her4* (*her4.1-her4.5* cluster probe), *her15* (*her15.1* and *her15.2* cluster probe), *her8a* and *her8.2* expression visualized by whole mount in situ hybridization (WISH). **(A-F)** 48 hpf WT sibling controls (*mib1*$^{+/+}$ or *mib1*$^{+/ta52b}$) and **(A'-F')** *mind bomb* mutant embryos (*mib1*$^{ta52b}$) which lack Notch activity. **(G-L')** Overactivated Notch signaling by heat-shock induced overexpression of the Notch intracellular domain (NICD) compared with heat shocked WT siblings at 72 hpf. **(M-R')** Notch inhibition by LY-411575 in 72 hpf larvae in comparison to DMSO controls. Larvae were treated from 64 to 72 hpf with 10 µM LY-411575 or 2% DMSO (controls), and fixed at 72 hpf. Sagittal optical sections at the midline are shown (lateral views, single DIC image planes, anterior at left, dorsal at top). Three larvae were imaged per condition and one representative image was selected. Scale bar, 100 µm. Abbreviations: pth, prethalamus; rh, rhombencephalon; tec, tectum; tel, telencephalon; th, thalamus proper. An anatomical reference scheme is provided in Fig. 2E.

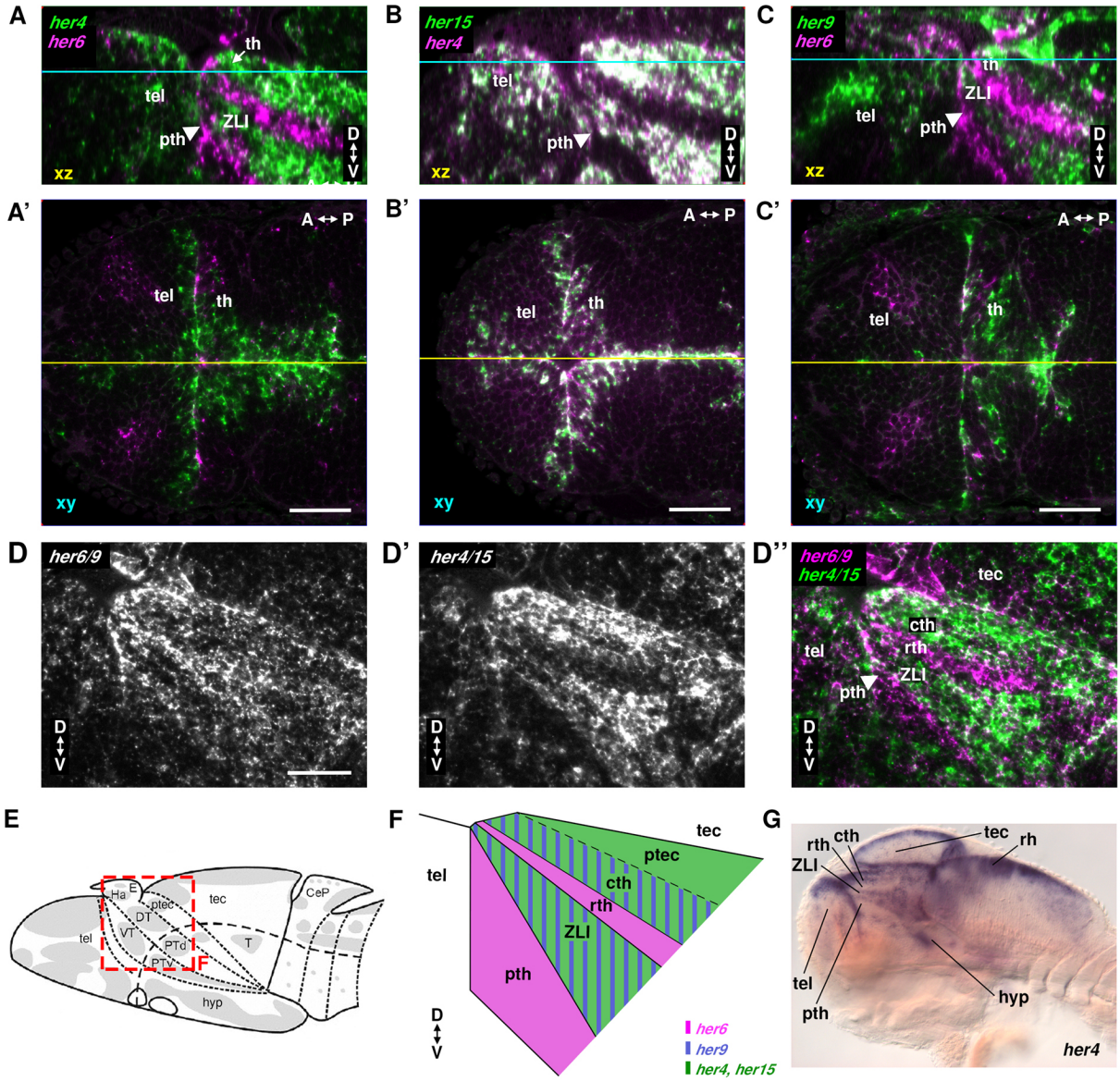


**Fig. 2. Co-expression analysis of *her* genes in the thalamus of 3 dpf larvae.**
**(A-D'')** Confocal imaging of double-fluorescent WISHs at 3 dpf. **(A, A')** Expression of *her4* (green) and *her6* (magenta). **(B, B')** Expression of *her15* (green) and *her4* (magenta). **(C, C')** Expression of *her9* (green) and *her6* (magenta). A, B and C are lateral views of midline sagittal orthogonal reconstructions of dorsal view (horizontal) stacks (levels indicated by yellow line in A', B' and C' respectively). A', B' and C' are dorsal views with the optical horizontal section level indicated in cyan in A, B and C. **(D-D'')** Lateral views of combined *her6/her9* (D'' magenta and D white, *her6* and *her9* probes mixed) and combined *her4/her15* (D'' green and D' white, *her4* and *her15* probes mixed) detection. D'' compares *her6/her9* to *her4/her15* expression. **(E)** Scheme of a 3 dpf zebrafish larval brain modified from (Mueller and Wullimann, 2016). Proliferation zones are indicated in grey. The dashed line separates the alar from basal plate. **(F)** Schematic map shows distinct domains of *her* gene expression at the ventricular wall of the alar diencephalon. Striped areas indicate that genes are co-expressed or expressing cells intermingled. **(G)** *her4* WISH in a 3 dpf larva with anatomical annotation, sagittal optical section. **(A-G)** The *her4* probe detects *her4.1-her4.5* and the *her15* probe detects *her15.1* and *her15.2*. All scale bars, 50 µm. Abbreviations: A-P indicates anterior-posterior orientation, D-V dorsal-ventral orientation. CeP, cerebellar plate; DT, dorsal thalamus proper, subdivided into rostral thalamus (rth) and caudal thalamus (cth); E,

epiphysis; Ha, habenula; hyp hypothalamus; ptec, pretectum; PTd, dorsal part of posterior tuberculum; pth, prethalamus; PTv, ventral part of posterior tuberculum; T, midbrain tegmentum; tel, telencephalon; tec, tectum opticum; VT, ventral thalamus or prethalamus (pth); ZLI, zona limitans intrathalamica.

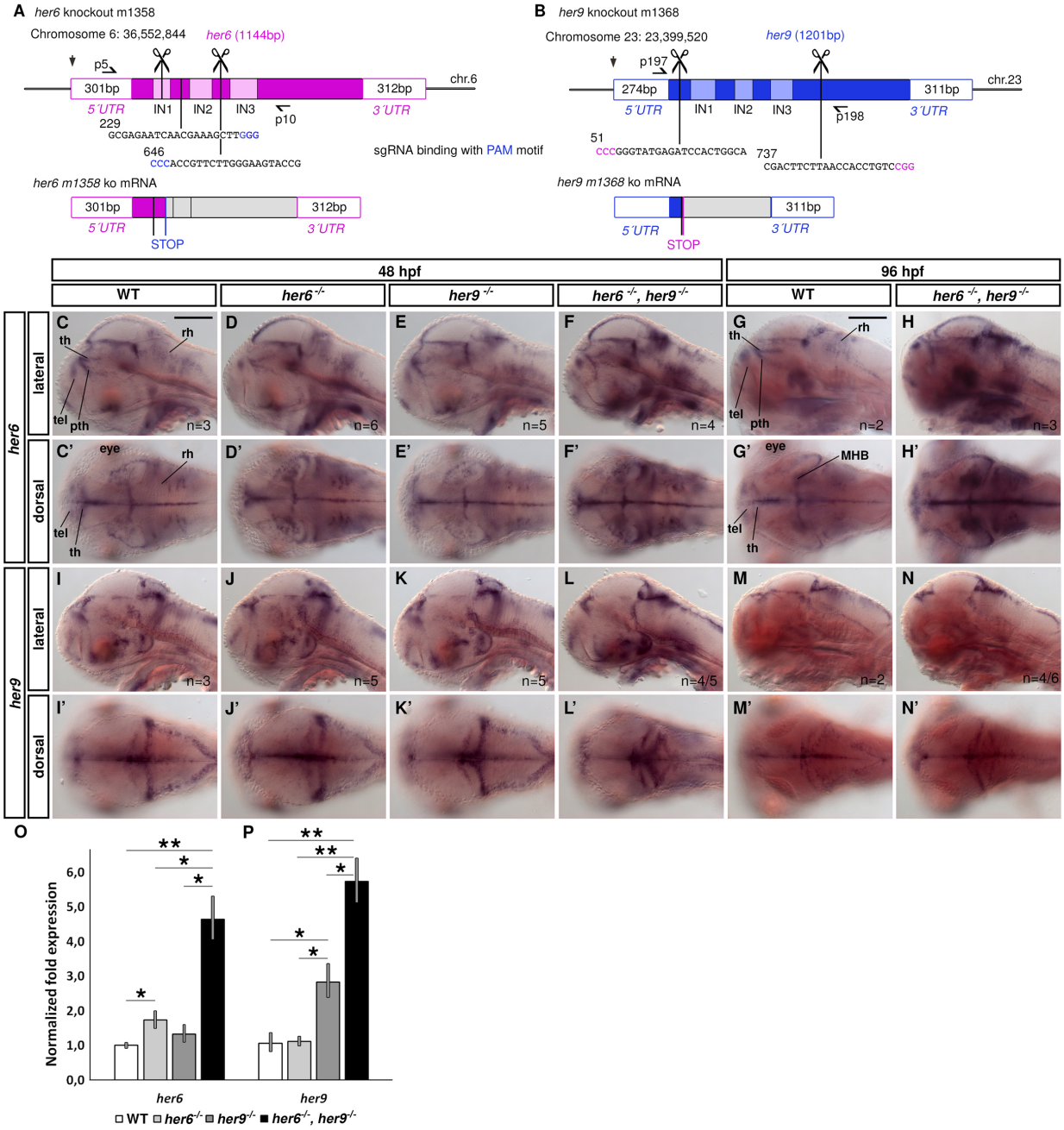


**Fig. 3. *her6* and *her9* single and double mutants reveal auto- and cross-regulation.** **(A, B)** Schematic for CRISPR/Cas9 deletion of the bHLH domains within the *her6* and *her9* genes, respectively. Straight vertical lines show the sgRNA binding sites. Scissors indicate the endpoints of the small deletion after non-homologous end joining. Half-arrows indicate primers (with names) which were used in genotyping PCRs. **(C-N')** WISH for *her6* **(C-H')** or *her9* **(I-N')** in WT (WT), *her6* and *her9* single or double mutants at indicated stages. (C-N) show lateral single sagittal optical plane images, (C'-N') dorsal views. Numbers of embryos analyzed are indicated in lower right corner. If different phenotypes were observed, n/n indicates numbers of embryos with phenotype shown in panel / total analyzed. Scale bars, 200 µm. **(O, P)** qPCR analysis of *her6* or *her9* expression in *her6* and *her9* single and double mutants. Error bars, SEM. Bars with asterisks indicate significant differences (* $p < 0.05$; ** $p < 0.01$; for exact values see Supplementary Table 5). Abbreviations: MHB, midbrain-hindbrain boundary; pth, prethalamus; rh, rhombencephalon; tel, telencephalon; th, thalamus proper.

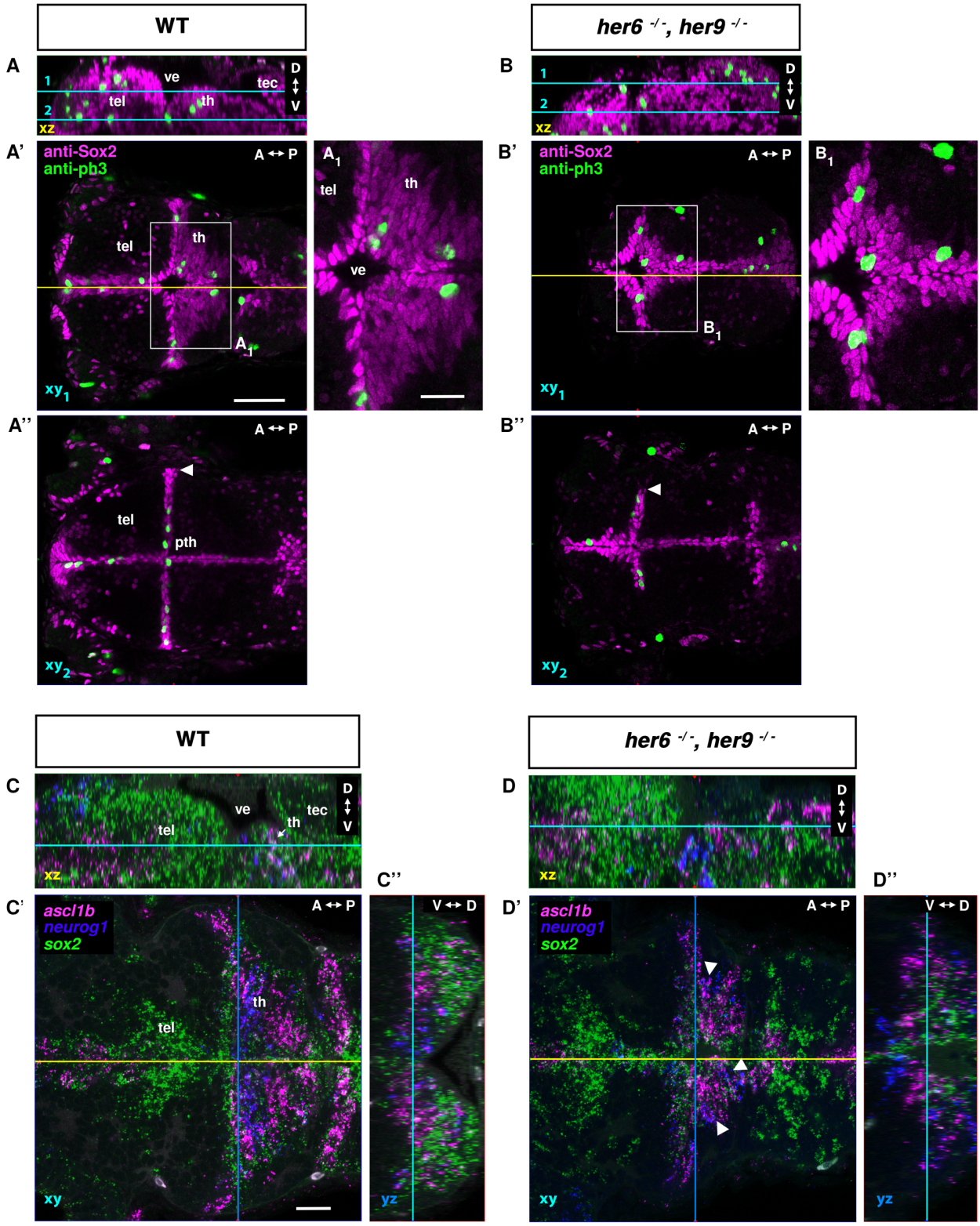


**Fig. 4. Neural stem and progenitor cell phenotypes in *her6*, *her9* double mutants.** **(A-B'')** Confocal image stacks of anti-Sox2 and anti-phospho-Histone H3 (pH3) immunofluorescence of 3 dpf WT control and *her6*, *her9* double mutants. **(A, B)** Lateral view midline sagittal XZ plane from orthogonal reconstructions, cyan lines indicating the dorsal view horizontal confocal planes 1 and 2 shown in A', A'' and B', B'', respectively. The yellow lines in A' and B' indicate the midline sagittal planes in A and B. Plane 1 in A' and B' shows the dorsal part of the diencephalon with the thalamus proper and plane 2 in A'' and B'' is located more ventrally including the prethalamus. $A_1$ and $B_1$ are magnifications of the boxed areas in A' and B'

respectively. Scale bar in A' (for A-A'', B-B'') is 50 µm; scale bar in $A_1$ (also for $B_1$) is 20 µm. The whole confocal stacks shown in A and B are also available as a combined Movie M2. **(C -D'')** Whole mount fluorescent hybridization chain reaction (HCR) for detection of *sox2* (green), *ascl1b* (magenta) and *neurog1* (blue) expression. **(C, D)** Midline sagittal views of orthogonal reconstructions with cyan lines indicating the dorsal view horizontal image planes in C' and D'. **(C', D')** Horizontal planes with blue lines indicate the level of frontal orthogonal reconstructions shown in C'' and D''. C'' and D'' are frontal views at the lateral expansion of the third ventricle. Scale bar in C', 20 µm. Numbers of embryos analyzed: A n=5; B n=4; C n=3; D n=3. Abbreviations: A-P indicates anterior-posterior, D-V dorsal-ventral orientation. pth, prethalamus; tec, tectum; tel, telencephalon; th, thalamus proper; ve, ventricle.

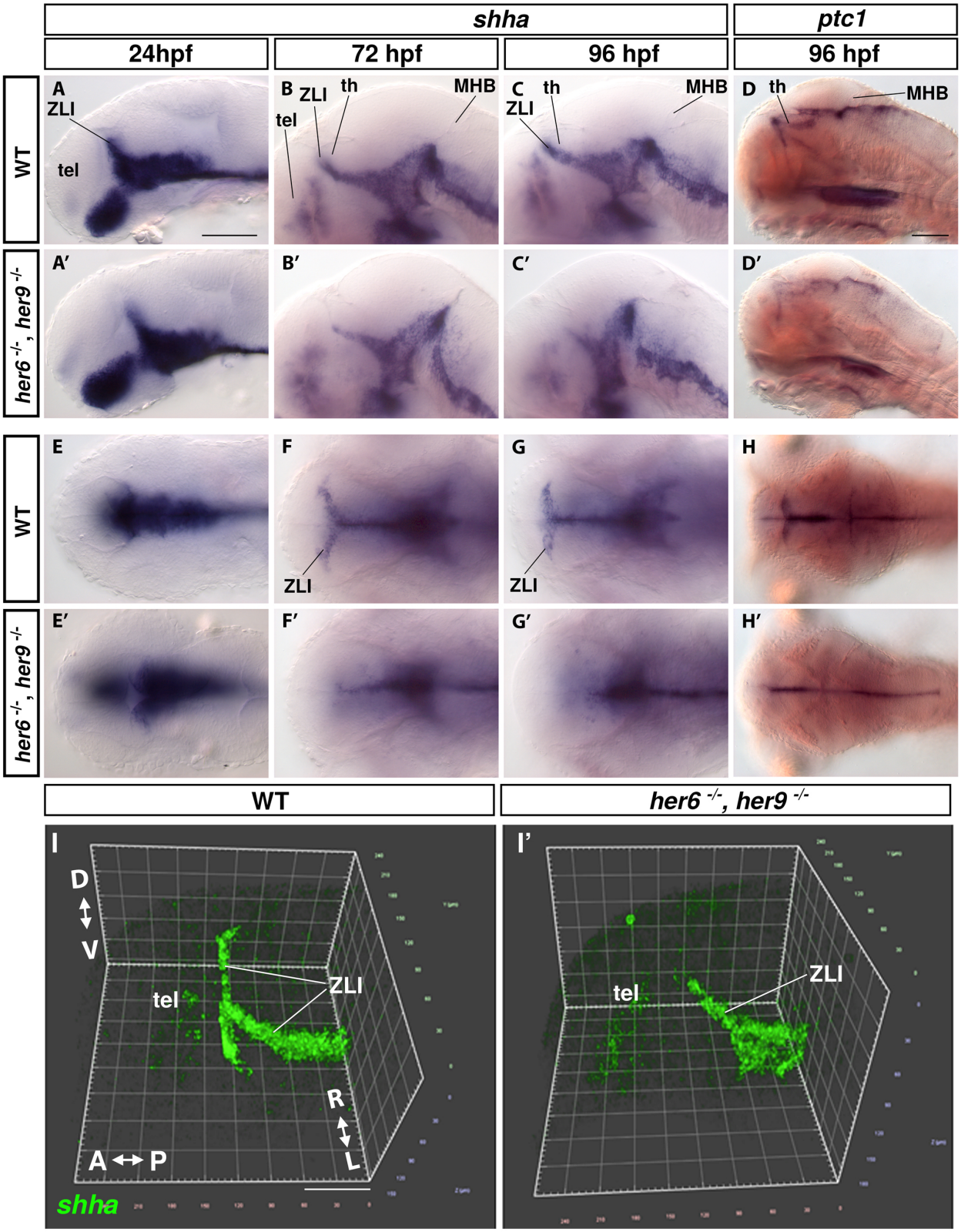


**Fig. 5. Loss of zona limitans intrathalamica *shha* expression in *her6*, *her9* double mutants.** **(A-H')** WISH showing *shha* (A-C', E-G') and *ptc1* (D, D', H, H') expression in WT and *her6, her9* double mutants. Genotypes are shown at left and the analyzed stages at top. **(A-D')** Lateral views show single sagittal image planes at the midline. **(E-H')** Dorsal views show single horizontal image planes at the level of the thalamus. Three larvae were imaged per condition and one representative image was selected. Expression of *shha* in *her6* and *her9* single mutants is shown in Fig. S9. Scale bar in A, 100 µm (for A-C' and E-G'); scale bar in D, 100 µm (for D, D', H, H'). **(I,**

**I')** 3D volume reconstruction of fluorescent WISH of *shha* in 3 dpf WT (I) and *her6*, *her9* double mutant (I'). Scale bar x-axis, 60 µm. A-P indicates anterior-posterior, D-V the dorsal-ventral, L-R the left-right orientation. Numbers of embryos analyzed: I n=3; I' n=4. Abbreviations: MHB, midbrain-hindbrain boundary; tel, telencephalon; th, thalamus proper; ZLI, zona limitans intrathalamica.

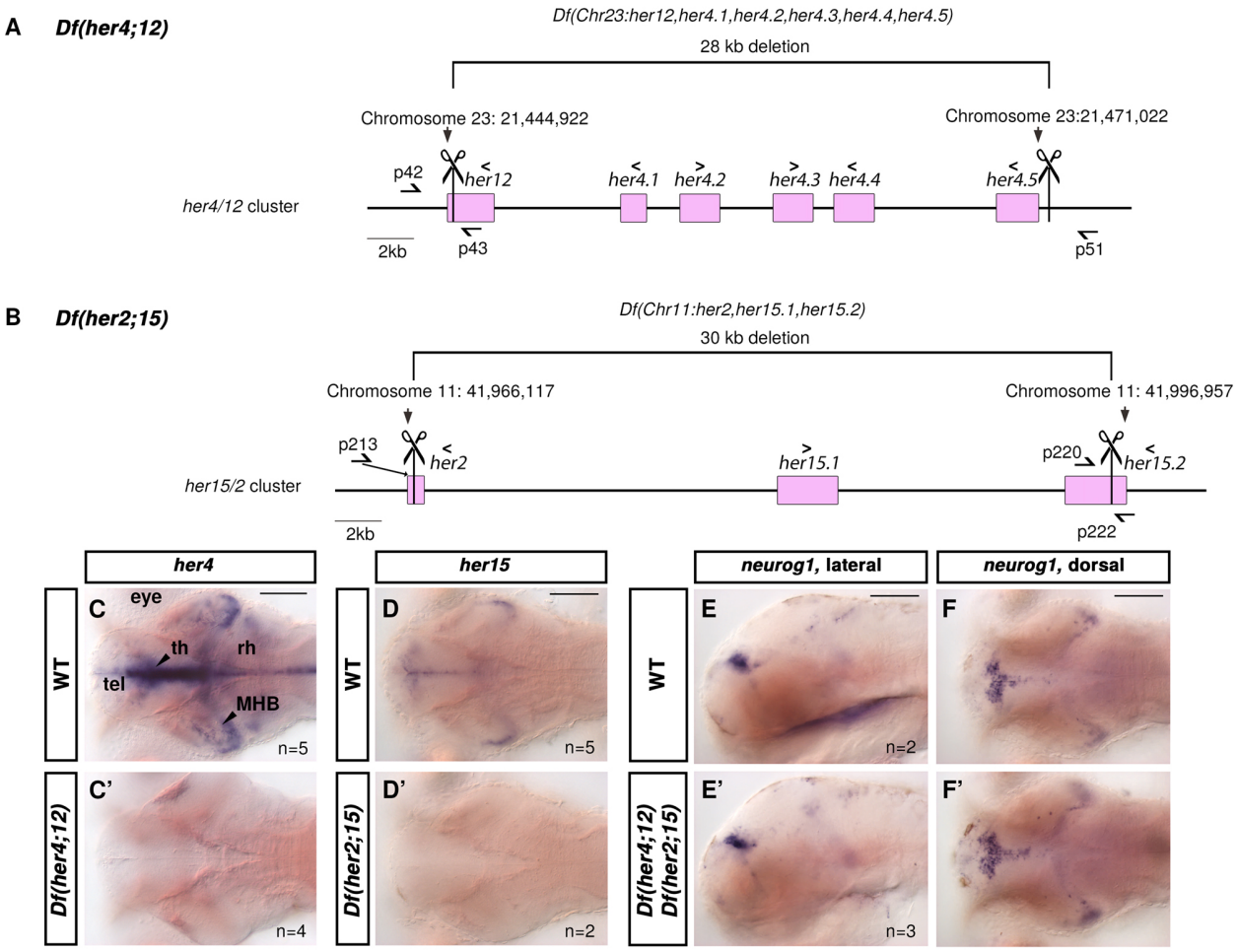


**Fig. 6. Genome editing strategy for *Df(her4;12)* and *Df(her2;15)* large chromosomal deletions: verification and *neurog1* expression.**

**(A, B)** Generation of large deficiencies using the CRISPR/Cas9 system. Scissors indicate the sgRNAs sequence positions, and square brackets indicate the deletion. 5'>3' or < signs indicate the orientations of all genes (pink boxes) in the intervals. Half-arrows indicate binding sites of primers used in genotyping PCRs (tagged with primer names). **(C-F')** WISH for *her4*, *her15* and *neurog1* mRNAs in 96 hpf larvae. No *her4* or *her15* signal is detectable in the respective mutants (C-D', dorsal view horizontal optical planes). No change in *neurog1* expression is detectable in *Df(her4;12)*, *Df (her2;15)* double deficiency mutants (E and E', midsagittal; F and F', horizontal optical sections). The *her4* probe detects *her4.1 to her4.*5 transcripts, and the *her15* probe detects *her15.1* and *her15.2* transcripts. Numbers of embryos analyzed are indicated in lower right corners. Abbreviations: MHB, midbrain-hindbrain boundary; rh, rhombencephalon; tel, telencephalon; th, thalamus proper. Scale bars, 100 µm.

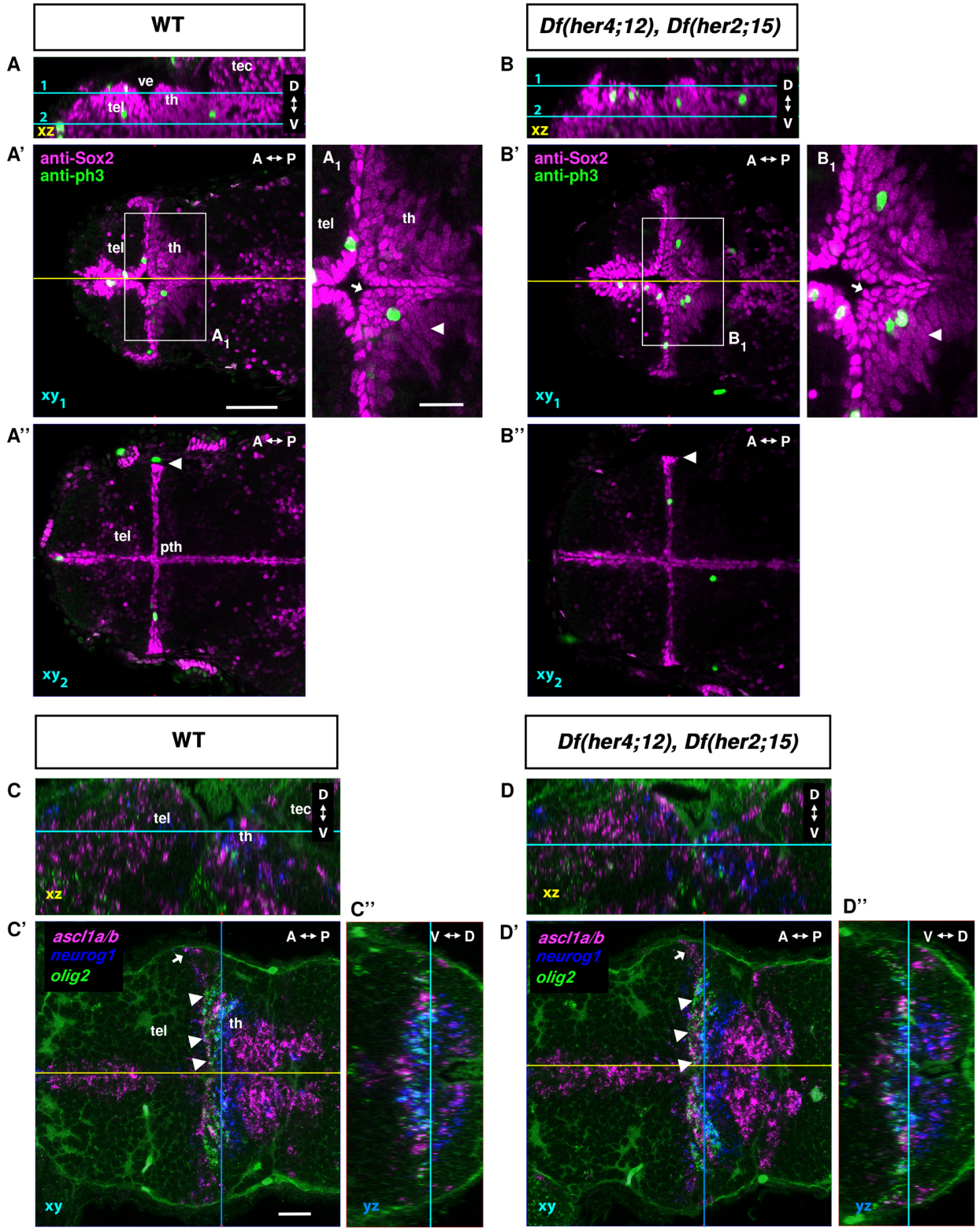


**Fig. 7. Sox2 and proneural gene expression in *Df(her4;12)*, *Df(her2;15)* double deficiency mutants.**

**(A-B'')** Confocal image stacks of anti-Sox2 and anti-pH3 immunostaining in 3 dpf WT **(A)** and *(her4;12)*; *Df(her2;15)* double deficiency mutants **(B)**. **(A, B)** Sagittal midline XZ plane from orthogonal reconstructions, cyan lines indicating the dorsal view confocal planes 1 and 2 shown in A', A'' and B', B''. The yellow lines in A' and B' indicate the midline sagittal planes in A and B. Plane 1 in A' and B' shows the dorsal part of the diencephalon with the thalamus proper and plane 2 in A'' and B'' is located more ventrally showing the prethalamus. $A_1$ and $B_1$ are magnifications

of the boxed area in A' and B', respectively. Scale bar in A', 50 µm (for A-B''); scale bar in $A_1$, 20 µm (also for $B_1$). The complete confocal stacks of larvae shown in A and B are combined in Supplementary Movie M3**. (C-D'')** Whole mount fluorescent HCR mRNA detection for *olig2* (green), *neurog1* (blue) and *ascl1a/b* (magenta) in **(C-C'')** WT and **(D-D'')** *Df(her4;12)*; *Df(her2;15)* double deficiency mutants. **(C, D)** Sagittal midline XZ plane from orthogonal reconstructions, with cyan lines indicating the confocal planes in C' and D'. **(C', D')** Dorsal view horizontal confocal planes of the diencephalon. Blue lines indicate the frontal view orthogonal reconstruction shown in C'' and D''. Numbers of embryos analyzed: A n=4; B n=5; C n=3; D n=3. Scale bar in C', 20 µm. Abbreviations: A-P indicates anterior-posterior, D-V dorsal-ventral orientation. pth, prethalamus; tec, tectum; tel, telencephalon; th, thalamus proper; ve, ventricle.

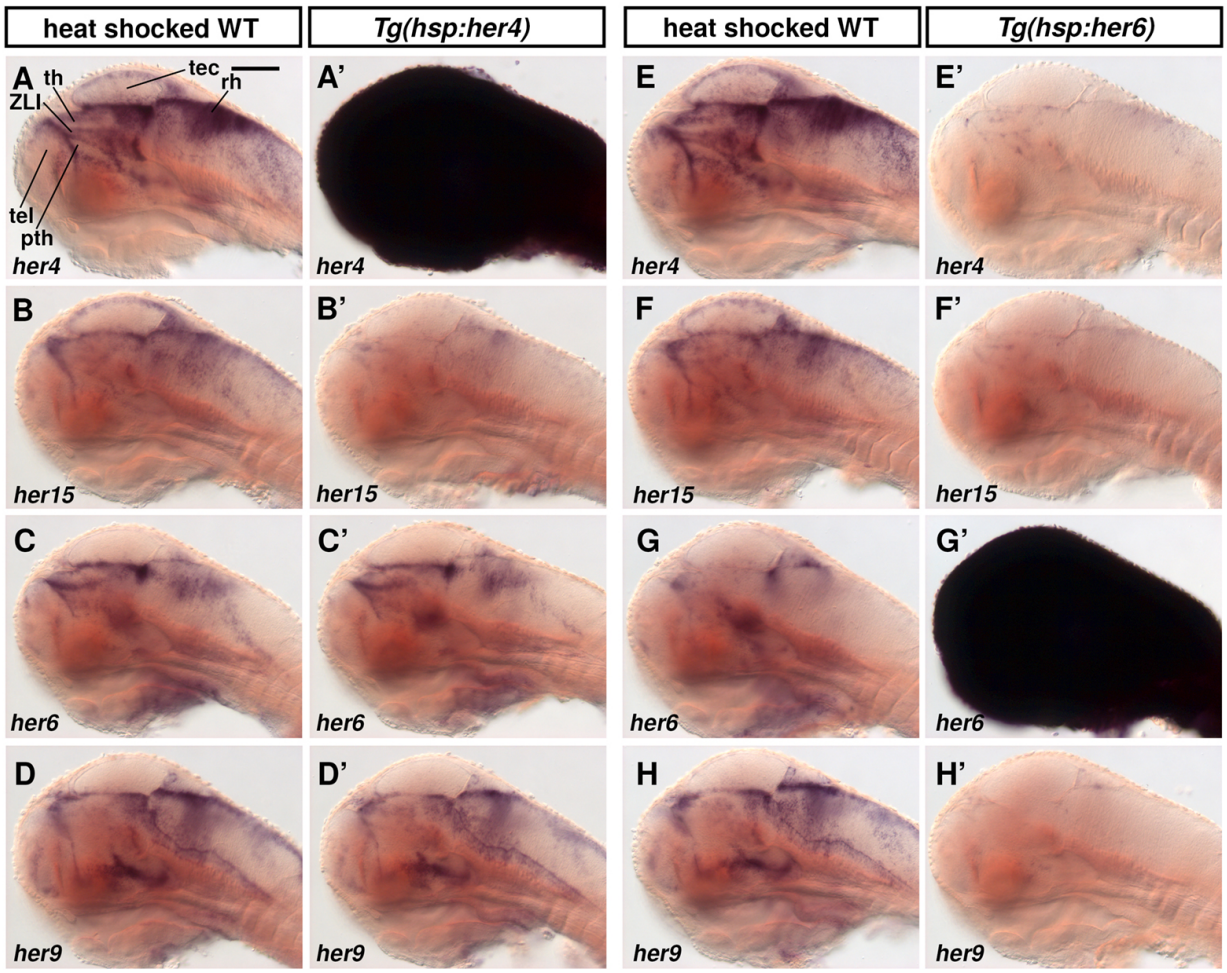


**Fig. 8. Overexpression of Her4 and Her6 reveals differential cross-regulation of *her* genes.** **(A-H')** WISH for *her* gene expression after heat shock induced overexpression of Her4 or Her6 in *Tg(hsp:her4-FLAG)* **(A'-D')** and *Tg(hsp:her6-FLAG)* **(E'-H')** transgenic embryos. **(A-H)** WT heat shocked sibling controls. A' and G' validate heat shock mediated high expression of *her4-FLAG* and *her6-FLAG* transgene transcripts. All larvae were heat shocked at 70 hpf for 30 min and were fixed at 72.5 hpf, except for G and G' that were fixed at 71.5 hpf because *her6* transcript levels decrease faster after heat shock than *her4* transcript levels (Sigloch and Driever, unpublished). Three larvae were imaged per condition and one representative image is shown. The *her4* probe detects *her4.1-her4.5* and the *her15* probe detects *her15.1* and *her15.2*. Sagittal optical sections close to midline, anterior at left, dorsal up; scale bar, 100 µm. Abbreviations: pth, prethalamus; rh, rhombencephalon; tec, tectum; tel, telencephalon; th, thalamus proper; ZLI, zona limitans intrathalamica.

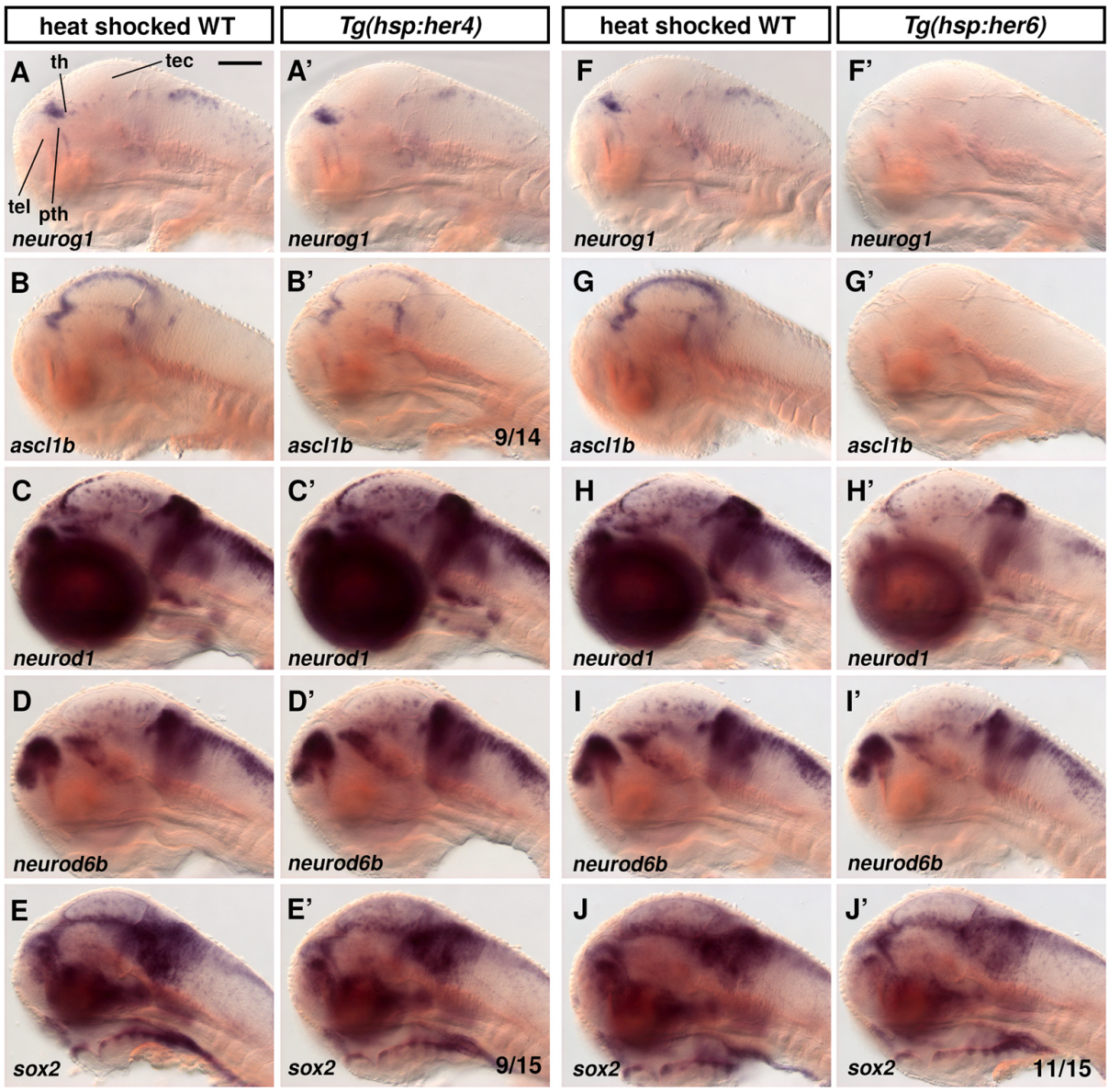


**Fig. 9. Overexpression of Her4 and Her6 differentially affect proneural gene expression.** **(A-J')** Expression of proneural genes and *sox2* after heat shock induced overexpression of Her4 or Her6. **(A'- E')** *Tg(hsp:her4-FLAG) and* **(F'-J')** *Tg(hsp:her6-FLAG)* were used to overexpress Her4 or Her6 by heat shock at 70 hpf for 30 min, and embryos were fixed at 72.5 hpf. (**A-J)** WT siblings were heat shocked as controls. For numbers of embryos analyzed see Supplementary Table 4. Analyzed conditions showed consistent WISH expression patterns in all embryos except B', E' and J', for which the most representative patterns are shown and their numbers out of total analyzed provided in bottom right of these panels. Sagittal optical sections close to midline, anterior at left, dorsal up; scale bar, 100 µm. Abbreviations: pth, prethalamus; tec, tectum; tel, telencephalon; th, thalamus proper.

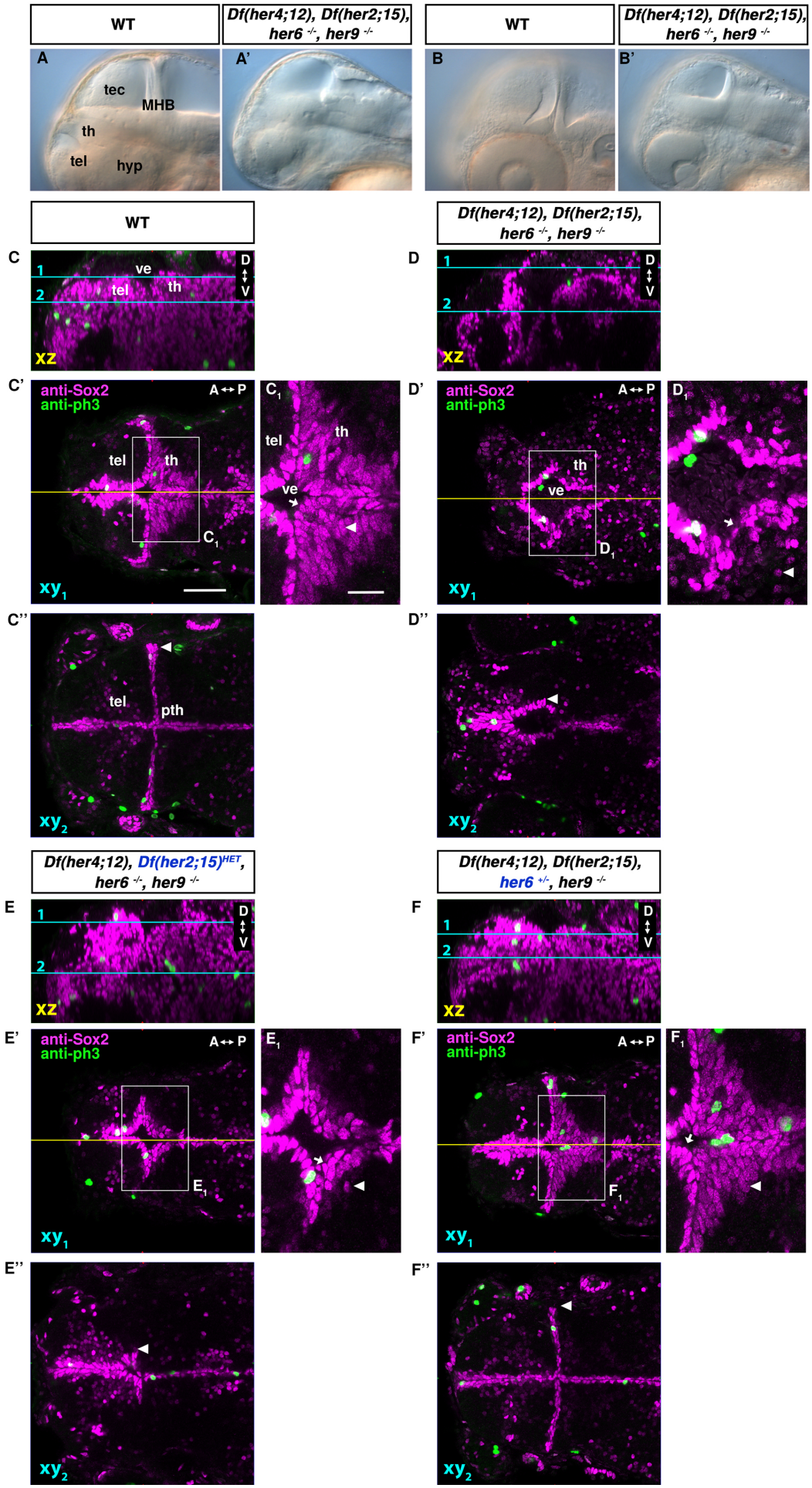
WT
Df(her4;12), Df(her2;15), her6 -/-, her9 -/-
A
A'
B
B'
tec
MHB
th
tel
hyp
C
D
1
2
ve
tel
th
D
V
xz
C'
D'
anti-Sox2
anti-ph3
A ↔ P
C1
D1
xy1
C''
D''
pth
xy2
Df(her4;12), Df(her2;15)HET, her6 -/-, her9 -/-
Df(her4;12), Df(her2;15), her6 +/-, her9 -/-
E
F
E'
F'
E1
F1
E''
F''

1276

1277 **Fig. 10. Analysis of the *her* activity depleted *her*UDM mutant phenotype.**
1278 **(A-B')** Live phenotype of WT and *Df(her4;12)*, *Df(her2;15), her6, her9* combined mutant
1279 (*her*UDM) embryos, lateral views at 56 hpf; (A) midsagittal optical section, (B) parasagittal optical
1280 section at level of lens. **(C-F'')** Anti-Sox2 and anti-pH3 immunofluorescence in 3 dpf WT **(C-C'')**
1281 and *her*UDM combined mutant (D-F'') embryos as indicated. **(E-E'')** Triple *(her4;12)*, *her6, her9*
1282 mutant *Df(her2;15)* heterozygous embryos showing minimal rescue of *her*UDM by one copy of
1283 the WT chromosomal region including *her2, her15.1, her15.2*. **(F-F'')** Triple *(her4;12)*,
1284 *Df(her2;15), her9* mutant and *her6* heterozygous embryo revealing efficient rescue of *her*UDM by
1285 one intact *her6* allele. **(C, D, E, F)** Mid-sagittal optical sections generated from orthogonal
1286 reconstruction of confocal stacks, cyan lines indicating the horizontal confocal planes 1 and 2
1287 shown in C', C'', D', D'', E', E'' and F', F''. The yellow lines indicate the sagittal midline sections
1288 shown in C, D, E and F. Plane 1 in C', D', E' and F' shows the dorsal part of the diencephalon and
1289 plane 2 in C'', D'', E'' and F'' is located more ventrally. $C_1$, $D_1$, $E_1$ and $F_1$ are magnifications of
1290 the respective boxed areas. A-P indicates anterior-posterior, D-V dorsal-ventral orientation. Scale
1291 bar in C' 50 µm for C-F''; scale bar in $C_1$ 20 µm for $C_1$-$F_1$. The confocal stacks in C and D as well
1292 as in E and F are provided as combined Supplementary Movies M4 and M5. Numbers of embryos
1293 analyzed: A n=1 (WT); A' n=3; C n=4; D n=4, E n=3 (in Fig. 10E, a *her2, her15* heterozygous
1294 larva is shown. Two more imaged larvae were WT for *her2, her15*), F n=4 (in Fig. 10F, a *her6*
1295 heterozygous larva was used. Three more imaged larvae were WT for *her6*). Abbreviations: hyp,
1296 hypothalamus; MHB, midbrain-hindbrain boundary; pth, prethalamus; tel, telencephalon; th,
1297 thalamus proper; ve, ventricle.
1298
1299

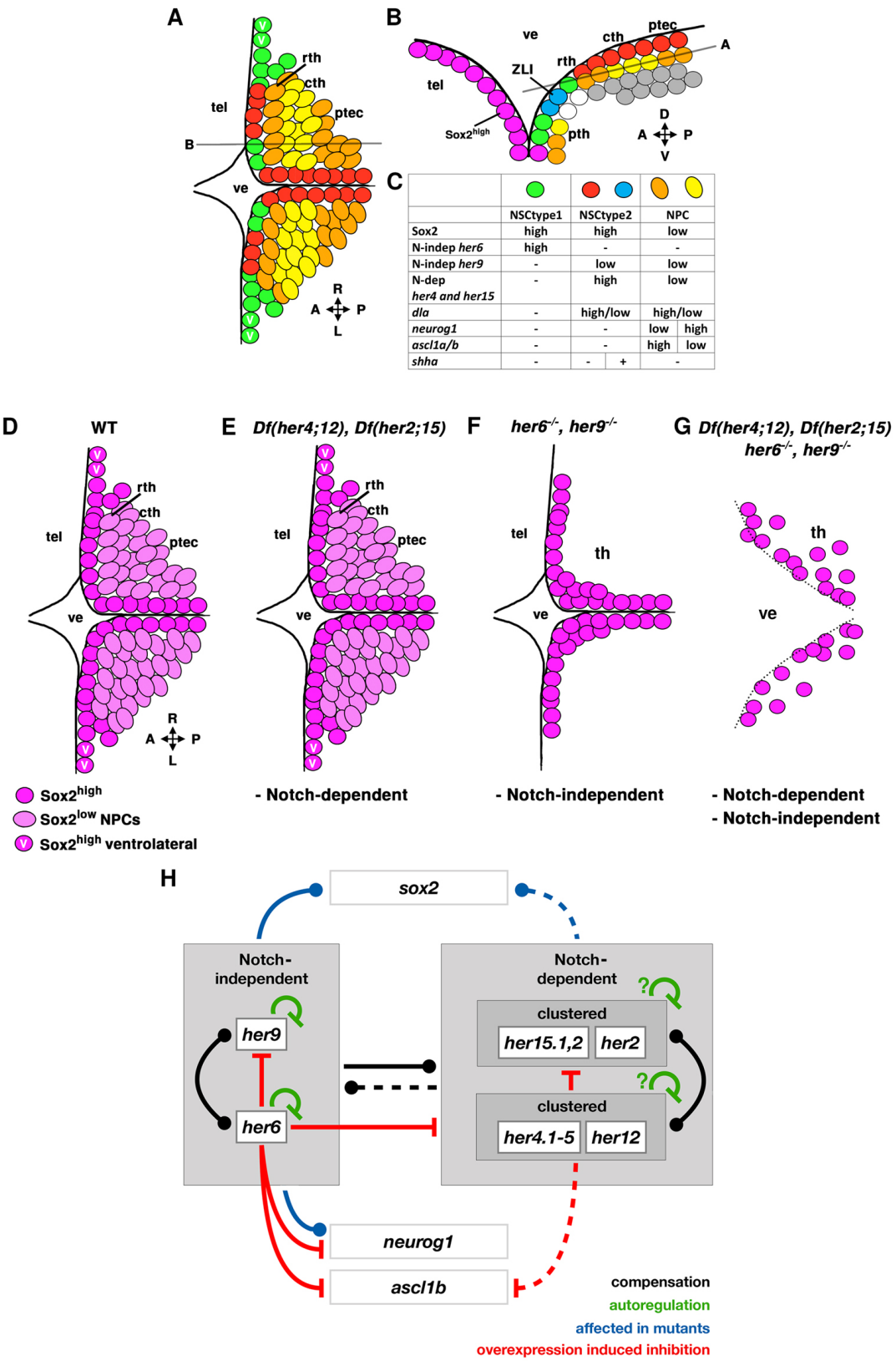


| | NSCtype1 | NSCtype2 | NPC |
|---|---|---|---|
| Sox2 | high | high | low |
| N-indep *her6* | high | - | - |
| N-indep *her9* | - | low | low |
| N-dep *her4 and her15* | - | high | low |
| *dla* | - | high/low | high/low |
| *neurog1* | - | - | low / high |
| *ascl1a/b* | - | - | high / low |
| *shha* | - | - / + | - |

**Fig. 11. Model of the cellular organization, observed *her* deficient phenotypes and model for *her* genetic interactions in the TPZ.**

**(A-C)** Model of cellular organization in the TPZ. (A) Horizontal plane dorsal view, plane indicated in (B), which shows parasagittal section as indicated in (A). The table in panel C indicates marker gene expression in different color-coded cell populations identified. Cells expressing *her6* are categorized as NSCtype1; Sox2$^{high}$ cells expressing *her4* and *her15* are categorized as NSCtype2 and expression of *neurogenin1* and *ascl1a/b* mark NPCs. Magenta cells are high Sox2 expressing

cells of the telencephalic ventricular wall, *her* expression not determined. White cells were not analyzed for expression of markers. Grey cells summarize differentiating early and mature neurons, some of which express *neurod* family members.

**(D-G)** Schematic of TPZ Sox2 expression in WT and different *her* combined mutant larvae. Cells (NSCs) with higher Sox2$^{high}$ levels are shown in dark magenta, and NPCs with lower Sox2$^{low}$ levels in light magenta. Cells with high Sox2 levels (and *her6* levels) that are only present in a more lateral and ventral region close to the lateral wall of the third ventricle are shown as magenta cells labelled "V". Black lines indicate the ventricular surface. **(D)** Schematic distribution of Sox2 in WT larvae. **(E)** Sox2 expression appears unchanged in the *Df(her4;12)*, *Df(her2;15)* double deficiency mutants. **(F)** *her6*, *her9* double mutants lack Sox2$^{low}$ expressing early neurogenesis progenitors and lack ventrally located Sox2$^{high}$ cells in the lateral walls of the third ventricle. **(G)** *her*UDM larvae, in addition to the *her6*, *her9* double mutant phenotype, show Sox2$^{high}$ nuclei scatter away from the ventricular surface. The dotted line suggests that the integrity of the ventricle is impaired.

**(H)** Postulated *her* gene network interactions. Boxes show analyzed genes and gene expression. Lines indicate how mutations or overexpression influence expression of other genes, interactions may not be direct. Black lines indicate which *her* genes may compensate for other *her* gene activity (dot indicates directionality). The dashed black line indicates genes that only partially rescue loss of *her6* and *her9*. Green inhibition signs illustrate the autoregulation of *her6* and *her9*, and postulated negative autoregulation in the *her4/her12* and *her15/her2* clusters. Blue influence signs show changed gene expression of Sox2 and *neurog1* in *her6, her9* double mutants. The blue dashed influence sign indicates that loss of Notch-dependent *her* activity in *Df(her4;12)*, *Df(her2;15)* only affects Sox2 expression when combined with the absence of *her6* and *her9* activity as detected in *her*UDMs. Red inhibition signs denote the downregulation of other genes upon overexpression of *her6* or *her4*. The dashed red inhibition signal indicates only mild downregulation of *ascl1b* by *her4* overexpression.

Abbreviations: A, anterior; P, posterior; L, left; R, right; D, dorsal; V, ventral; cth, caudal thalamus; ptec, pretectum; pth, prethalamus; rth, rostral thalamus; tel, telencephalon; ve, ventricle; ZLI, zona limitans intrathalamica.